NASA CR 120828
BC-8367-FR

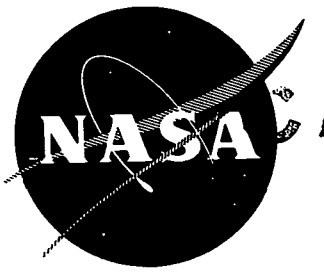

FILAMENT-WOUND, FIBERGLASS CRYOGENIC TANK SUPPORTS

by

J. S. Carter and T. E. Timberlake

BRUNSWICK CORPORATION

prepared for

NATIONAL AERONAUTICS AND SPACE ADMINISTRATION

NASA Lewis Research Center
Contract NAS3-14627
Brad Linscott, Project Manager

NASA CR 120828
BC-8367-FR

FINAL REPORT

FILAMENT-WOUND, FIBERGLASS CRYOGENIC TANK SUPPORTS

by
J. S. Carter and T. E. Timberlake

BRUNSWICK CORPORATION
Technical Products Division
4300 Industrial Ave.
Lincoln, Nebraska 68504

prepared for

NATIONAL AERONAUTICS AND SPACE ADMINISTRATION

September 15, 1971

Contract NAS3-14627

NASA Lewis Research Center
Cleveland, Ohio
Brad Linscott, Project Manager
Advanced Systems Division

FOREWORD

The work described herein was performed by the Technical Products Division of the Brunswick Corporation under National Aeronautics and Space Administration Contract NAS3-14627. This final report covers the design, analysis, fabrication, test and delivery of cryogenic tank supports. The work was performed under the direction of the NASA Project Manager, Mr. Brad Linscott, Advanced Systems Division, NASA-Lewis Research Center.

TABLE OF CONTENTS

LIST OF TABLES

LIST OF ILLUSTRATIONS

ABSTRACT

This report describes the design, fabrication and testing of filament-wound, fiberglass cryogenic tank supports for a LH_2 tank, a LF_2/FLOX tank and a CH_4 tank. These supports consist of filament-wound fiberglass tubes with titanium end fittings at each end. These units were satisfactorily tested at cryogenic temperatures, thereby offering a design that can be reliably and economically produced in large or small quantities. The basic design concept is applicable to any situation where strong, lightweight axial load members are desired.

FILAMENT-WOUND, FIBERGLASS CRYOGENIC TANK SUPPORTS

by James S. Carter and Thomas E. Timberlake
Brunswick Corporation

SUMMARY

The objective of this program was to design, fabricate, and qualify filament-wound cryogenic tank support struts that would:

1. Withstand the axial tension and compression loads at both ambient and cryogenic temperatures.

2. Be economical to produce in large or small quantities, with inherent high reliability and reproducibility characteristics.

Three different support struts were designed, fabricated, and tested for this program: One each for the LH_2 tank, LF_2/FLOX tank, and Liquid CH_4 tank. The struts consisted of fiberglass tubes with titanium end fittings into which spherical rod end bearings were threaded to support the cryogenic tanks.

The most significant design feature was the utilization of a continuous fiberglass-to-fitting joint for transferring axial loads from the fiberglass tube to the end fittings. This mechanical joint does not depend upon an adhesive bond, and therefore provides a greater degree of structural strength.

Fabrication techniques included the use of a standard helical winding machine which controlled fiber orientation accurately and precisely. "Hand lay-up" operations were minimized. In these combined manners, a high degree of manufacturing consistency was attained, thereby optimizing reliability and reproducibility characteristics.

INTRODUCTION

Cryogenic tank support systems must withstand the cryogenic temperatures of liquid hydrogen, liquid methane, and cryogenic oxidizers such as oxygen and flourine, while providing structural and thermal radiation barrier characteristics compatable with mission requirements. The program objective was to design and build lightweight filament-wound tank supports that would be thermally and structurally efficient for each of the three cryogens listed above.

This program encompassed design, material selection, fabrication, tooling concepts, and testing of three support configurations for

subsequent static tests for NASA under systems environmental conditions. The thermal design and cryogenic testing was performed by the Hauser Research and Engineering Company, Boulder, Colorado. A report on this investigation is presented in Appendix A of this report.

The final design consisted of a filament-wound fiberglass tubular section with integral titanium end fittings. Thermal radiation barrier material, consisting of chopped Dexiglass and aluminized mylar, was inserted in the support. Spherical rod end bearings were threaded into each end for attachment to the cryogenic tank and support frame.

Five experimental supports were fabricated to verify the design, fabrication technique, and the structural integrity. These supports were retained by the Brunswick Corporation.

Sixteen supports of each configuration were fabricated for NASA. Three supports from each set of sixteen were structurally tested to destruction. These tests verified that the supports exceeded the structural loading at cryogenic temperature as specified by NASA. The remaining supports were subjected to non-destructive proof loads at room temperature, prior to delivery to NASA.

DESIGN, FABRICATION AND TEST

Design

The overall objective of the design effort was to obtain a lightweight strut for cryogenic service that would be structurally reliable, have a low thermal heat conductance, and could be economically produced in small or large quantities. The strut assembly which meets this objective consists of a filament-wound fiberglass tubular section with integral titanium end fittings. The titanium end fittings have a threaded hole into which spherical rod end bearings are threaded. A special thermal radiation barrier is inserted into the tube (through the threaded hole) prior to installation of the rod end bearings. A drawing of the assembled strut is shown in Figure 1. Photographs of the three assembled struts (LH_2 tank, LF_2/FLOX tank, and Liquid CH_4 tank) are shown in Figures 2, 3, and 4. Table I shows the weight breakdown of the production strut assemblies.

Details of the structural design will be discussed in the following order: Fiberglass-to-fitting joint, wind pattern, wall thickness, titanium end fitting design, and thermal design and analysis. Table II lists the ultimate structural design loads at cryogenic temperature.

Figerglass-to-fitting joint - The prime consideration in the joint design was to provide a joint that (1) would be as strong as the cylinder wall (2) could be fabricated inexpensively, and (3) would achieve reproducible test results. In response to these requirements Brunswick selected a joint concept that does not rely on an adhesive bond between the fiberglass and the end fitting. The reaction of tensile load is achieved by designing the outer contour of the end fitting as a geodesic isotensoid surface. The tensile load is reacted by an isotensoid stress in the helical winding similar to the way a geodesic isotensoid dome reacts pressure in a pressure vessel.

The compression load capability is built into the joint by reinforcing the helical winding in the dome with unidirectional 143 Cloth and circumferential filament windings so that the compression load can be transferred from the cylinder wall to the fitting flange. The 143 Cloth is orientated with the principal strength in the longitudinal direction. This design concept achieves a simple, lightweight, one-piece joint that can be easily and reliably manufactured.

In tests, the joint developed sufficient strength to always fail the cylinder wall. The maximum wall stresses obtained were 65,811 Newtons/cm^2 (95,448 psi) tension and 37,336 Newtons/cm^2 (54,150 psi) in compression (buckling failure). No attempt was made to further optimize the joint design because of the limited number of prototype tests scheduled prior to a design release for production.

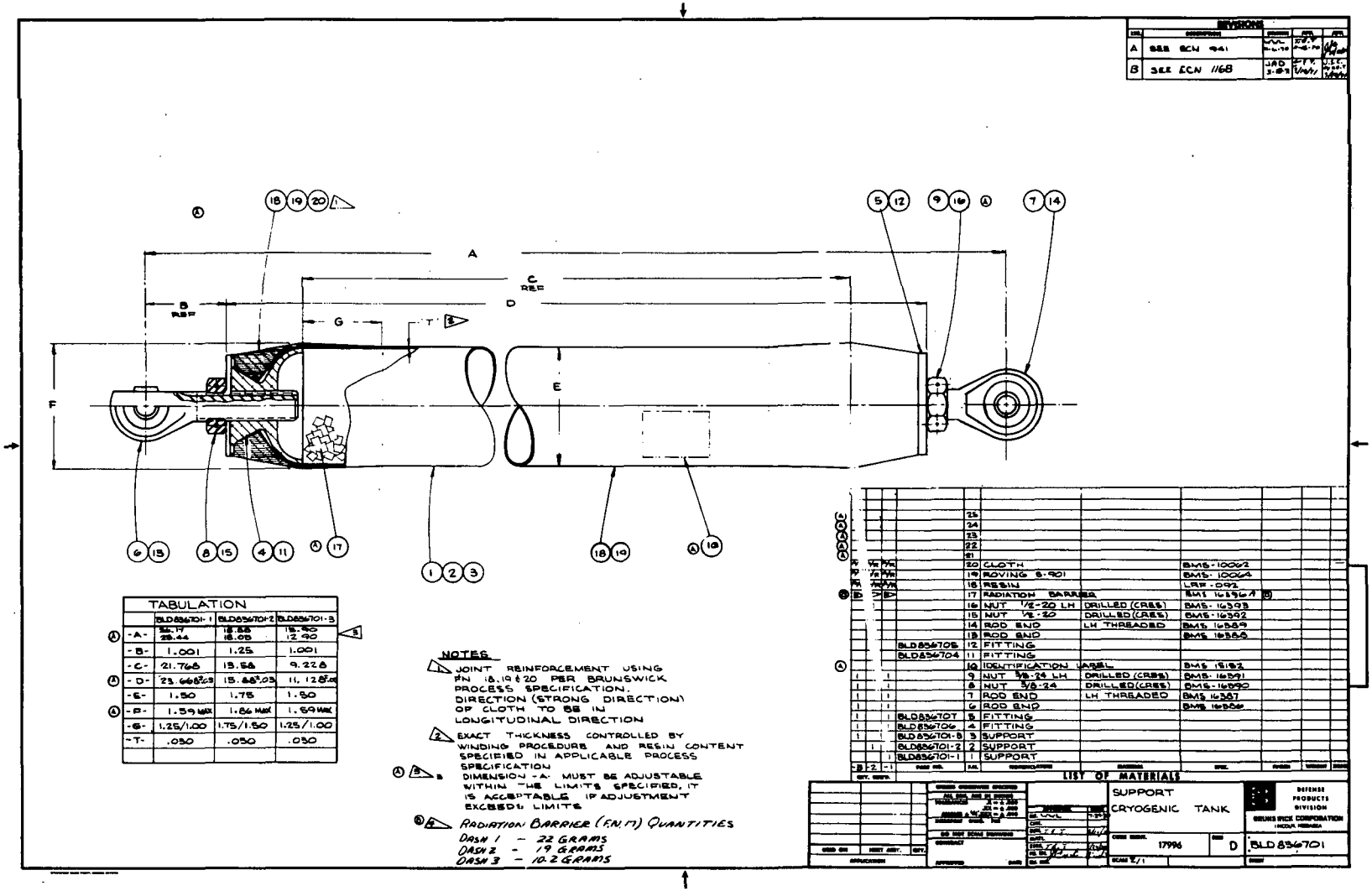

Figure 1. Support Assembly Drawing

Figure 2. Support Assembly for LH_2 Tank

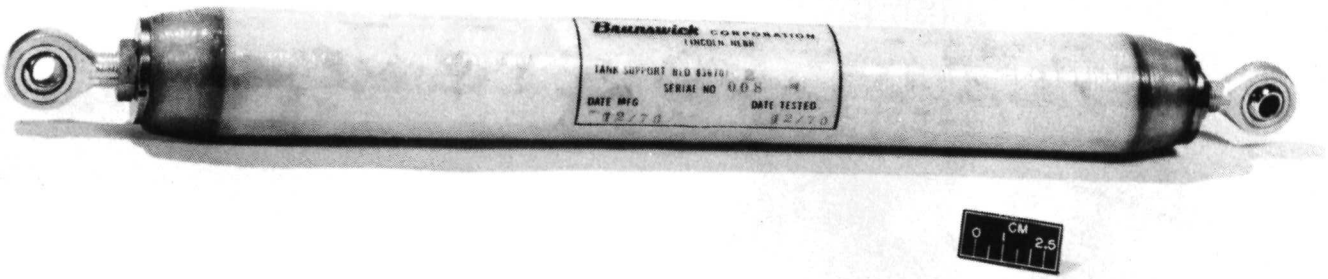

Figure 3. Support Assembly for LF_2/FLOX Tank

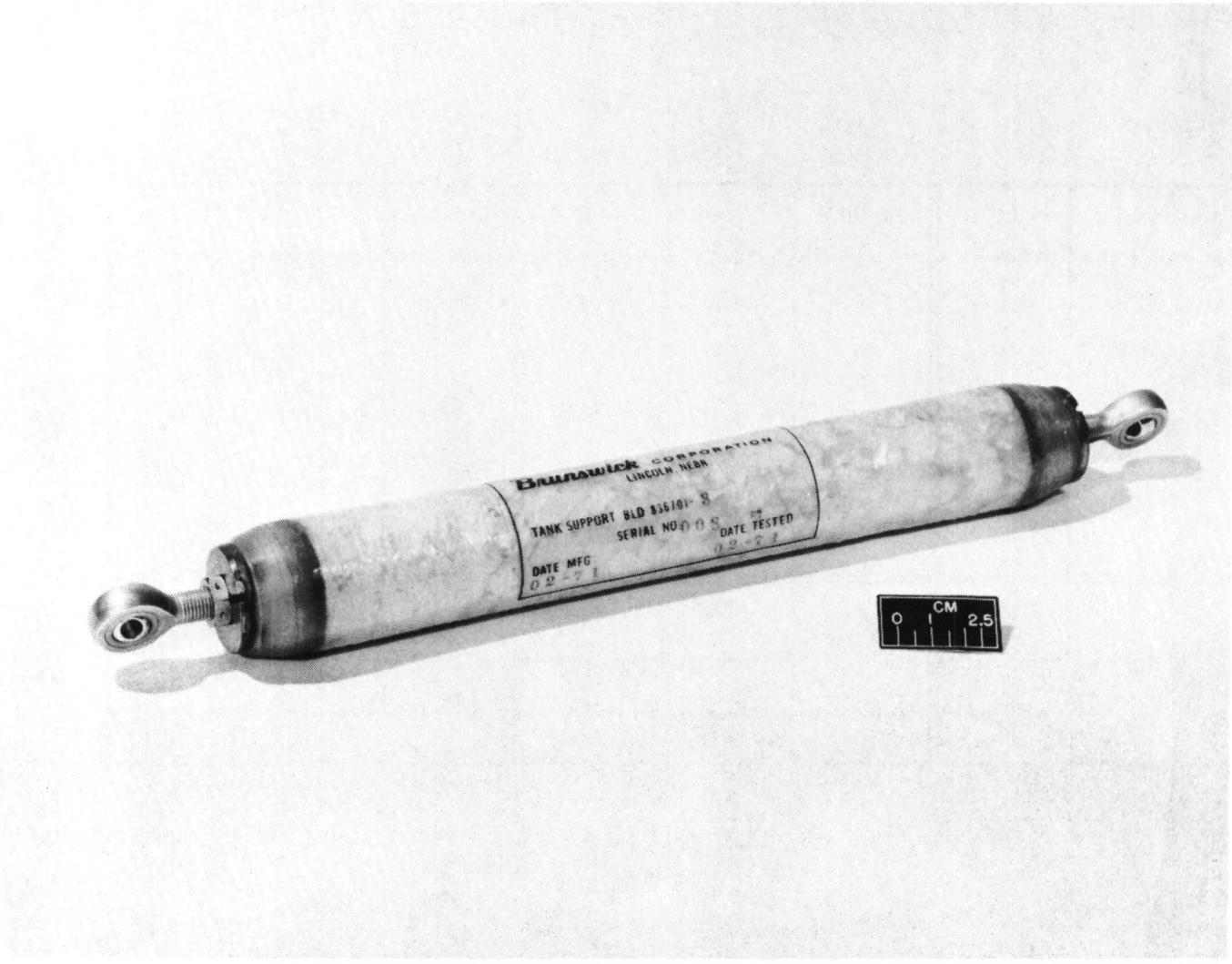

Figure 4. Support Assembly for CH_4 Tank

TABLE I WEIGHT BREAKDOWN OF STRUT ASSEMBLY

Component	BLD-836701-1			BLD-836701-2			BLD-836701-3		
	Weight		% of Total	Weight		% of Total	Weight		% of Total
	Grams	(lbs.)		Grams	(lbs.)		Grams	(lbs.)	
Fiberglass	159.2	.351	47.1	197.3	.435	38.03	91.6	.202	35.44
Titanium End Fittings	65.3	.144	19.33	118.8	.262	22.90	65.3	.144	25.26
Rod Ends	83.9	.185	24.83	166.0	.366	31.99	83.9	.185	32.46
Jam Nuts	7.3	.016	2.15	17.7	.039	3.41	7.3	.016	2.81
Thermal Barrier	22.2	.049	6.58	19.1	.042	3.67	10.4	.023	4.03
TOTAL	337.9	.745	100.00	518.9	1.144	100.00	258.5	.570	100.00

TABLE II DESIGN ULTIMATE LOADS AT CRYOGENIC TEMPERATURE

Tank Type	Part Number	Temperature				Tensile Load		Compression Load	
		Cold End		Warm End					
		°R	°K	°R	°K	Newtons	Lbs.	Newtons	Lbs.
LH_2	BLD-836701-1	37	20.55	400	222.22	6761	1520	5560	1250
Flox	BLD-836701-2	155	86.11	400	222.22	36,918	8300	25,087	5640
CH_4	BLD-836701-3	204	113.33	400	222.22	9919	2230	8318	1870

Wind pattern selection - The helical wind angles chosen for the three struts were the lowest angles that were compatible with the joint concept and helical winding practice. The limiting factor on the lower limit was the O.D. of the neck of the fitting which was determined by the size of the rod end specified by the procuring activity and the neck thickness required for fitting strength. Helical wind angles of 27° 49', 30° 26' and 25° 48' were selected for the three struts. Circumferential windings (90°) were added at a ratio of approximately one circumferential winding to two helical windings. The properties of the three wind patterns are shown in Table III.

Strength values in Table III were obtained from AFML-TR-66-274, "Testing Techniques for Filament Reinforced Plastics", Armed Forces Support Center, Washington, D.C. May 1964. 30° helical wind and 90° hoop wind at a 2/1 ratio was used. Values were adjusted for difference in bulk factor, (.909 reduction factor). The elastic modulii properties were calculated on Brunswick's computer program for the actual construction. The properties listed in Table III were calculated at room temperature conditions.

Selection of cylinder wall thickness - Column buckling was the design criteria for the selection of the wall thickness (outside diameter fixed) on the BLD-836701-1 and -2 struts. A wall thickness which resulted in a conservative margin of safety of +.74 and +.71 respectively was chosen for these two struts. A conservative margin of safety of column buckling was used because there was concern about the effect that small surface irregularities in a thin wall, .0762 cm (.030 inch) and .127 cm (.050 inch) respectively, might have on the column buckling results. The number of prototype tests scheduled were insufficient to obtain statistical data on column buckling.

The wall thickness of the BLD-836701-3 strut was sized the same as the -1 strut (.0762 cm). The .0762 cm (.030 inch) thickness was chosen because it was thought that if the wall was any thinner it might be too fragile and thus be susceptible to damage from handling. Tables IV, V and VI list the calculated design stresses, column buckling loads, local crippling stresses, and margins of safety for the three struts at room temperature conditions.

On the basis of the test results, which are discussed in the test section, it appears possible to reduce the wall thickness by 27%. This would yield a margin of safety on column buckling of +.25 for the -1 and -2 designs, and a margin of safety on compressive crippling of +.46 for the -3 design. The wall thickness for the three designs would be .0559 cm (.022 inch) respectively. There would be some question, however, if the .0559 cm (.022 inch) thickness would have sufficient ruggedness. If the 27% wall weight reduction was also affected in the fiberglass joint, the weight reduction for the three designs, as a percentage of the original total weight, would be respectively 12.72%, 10.27% and 9.57%.

Titanium end fittings - The titanium end fittings were conservatively designed so that an ultimate failure of the strut assembly would always occur in the fiberglass. This resulted in the titanium end fittings having nearly the same load capability as the threaded rod end bearings specified by the procurring activity. A closer design of the fitting could achieve a 15% to 30% weight reduction of the fitting which would result in a 3% to 6% weight reduction of the strut assemblies.

Thermal design and analysis - A thermal analysis of the three struts and the design of the internal thermal radiation barrier was accomplished during this program. This work was accomplished for the Brunswick Corporation by Dr. Ray L. Hauser of Hauser Research and Engineering Company, Boulder, Colorado. The complete thermal analysis report is presented in Appendix A, and includes the following:

1) Thermal conductivity values for glass/epoxy composite materials are identified.

2) The -1 strut for use with liquid hydrogen tanks was analyzed for heat conduction and internal radiation in a vacuum, coast condition. This strut was also analyzed for heat conduction and convection in a helium atmosphere. Temperature profile and heat transfer results are presented.

3) The -2 strut for use with flox tanks and the -3 strut for use with liquid methane were analyzed for heat conduction and convection in a helium atmosphere. Temperature profile and heat transfer results are presented.

4) A study was made of the internal radiation problem and a design for the radiation shielding was recommended and analyzed. The recommended design for the internal radiation barrier was a mixture of Dexter paper #1303 (13.74 gm/sq meter) and .25 mil aluminized mylar (9.12 gm/sq meter) at a weight ratio of 66.82% Dexter paper and 33.18 aluminized mylar. The amount of barrier recommended for the -1, -2 and -3 struts was 11 grams, 9.5 grams and 5.1 grams respectively.

   NASA Lewis performed acceleration tests on the -1 strut and discovered that settling of the radiation barrier occurred. As a result of these tests, NASA Lewis recommended the total radiation barrier be doubled by adding more Dexter glass. Their recommendation was followed. This resulted in a weight ratio of 87.54% Dexter glass #X1303 (13.74 gm/M2). The weight of the barrier mixture is 22 grams, 19 grams, 10.2 grams respectively for the -1, -2 and -3 struts.

   This change will have a negligible effect in the radiation heat transfer predicted in the report.

TABLE III STRUT CYLINDER WALL COMPOSITE PROPERITES

Part No.	Ratio of Helical Glass to Hoop Glass	Helical Wind Angle	Longitudinal Strength				Elastic Modulus			
			Tensile		Compressive		Longitudinal		Circumferential	
			$10^3 N/cm^2$	KSI	$10^3 N/cm^2$	KSI	$10^6 N/cm^2$	10^6PSI	$10^6 N/cm^2$	10^6PSI
836701-1	2.65	27°49'	84.8	123	59.3	86	2.781	4.033	2.253	3.268
836701-2	2.04	30°36'	84.8	123	59.3	86	2.487	3.607	2.495	3.618
836701-3	2.60	25°48'	84.8	123	59.3	86	2.942	4.267	2.264	3.284

TABLE IV CYLINDER WALL STRESS

Strut	Mean Radius		Wall Thickness		Design Load		Stress		Margin of Safety
	Cm	In	Cm	In	Newtons	Lbs.	N/cm^2	PSI	
836701-1	1.867	-735	.0762	.030	- 5560 + 6761	-1250 +1520	- 6223 + 7567	- 9025 +10,974	+ 8.52 +10.2
836701-2	2.159	.850	.127	.050	-25,087 +36,918	-5640 +8300	-14,571 +21,443	-21,133 +31,100	+ 3.07 + 2.94
836701-3	1.867	.735	.0762	.030	- 8318 + 9919	-1870 +2230	- 9309 +11,101	-13,501 +16,100	+ 5.36 + 6.63

TABLE V COLUMN BUCKLING

Strut	Length		Buckling Load		Design Load		Margin of Safety
	Cm	In	Newtons	Lbs	Newtons	Lbs	
836701-1	66.47	26.17	-9961	-2171	-5560	-1250	+ .74
836701-2	47.96	18.88	-42,785	-9619	-25,087	-5640	+ .71
836701-3	35.31	13.90	-36,215	-8142	-8319	-1870	+3.35

TABLE VI COMPRESSIVE CRIPPLING STRESS IN WALL

Strut	Compressive Crippling Stress		Design Stress		Margin of Safety
	N/cm^2	PSI	N/cm^2	PSI	
836701-1	-24,653	-35,755	- 6223	- 9025	+2.96
836701-2	-35,165	-51,000	-14,571	-21,133	+1.41
836701-3	-25,497	-36,979	- 9309	-13,501	+1.74

Fabrication

The tank supports were fabricated using filament-wound S-901 glass and epoxy resin over a water soluble mandrel. The mandrel consisted of a wind axis and water soluble sand core which was used to locate the end fittings and control the support configuration. A schematic of the mandrel assembly is shown in Figure 5.

The three configurations were processed under the same processing techniques with the only differences being length, diameter, and thickness of the strut. Thus, the processing sequence, as described in this section, will describe the general fabrication techniques for all struts with a summary of the differences at the end of this section. The fabrication steps are discussed in four sections as follows: mandrel assembly, materials, filament winding, and final assembly.

Mandrel assembly - The mandrel assembly was prepared as shown in Figure 5. A pre-molded sand mandrel was assembled onto a wind axis and one fitting (titanium) assembled on each end. The fittings were locked into position by inserts and retained by a jam nut on each end. The wind axis was used to locate the fittings and sand mandrel in the proper position for insertion into the filament winding machine. End fittings used for centers in the winder were then inserted and positioned by a set-screw on each end. These large diameter centers were required to improve stiffness of the small diameter rod (wind axis).

The assembled mandrel was inspected for proper length, quality, surface finish, etc., and released to production for fabrication.

Materials - The tank supports were fabricated using S-901 glass and epoxy resin for the tubular structure. Titanium fittings and rod end bearings were as required by NASA contract. A description of each material used in the construction of the tank support, including governing specification and suppliers, is presented below.

S-901 glass roving: The roving was purchased certified to MIL-R-60346, Type III, Class A in the form of 12-end S/G 140 from Owens Corning fiberglas.

S-glass Cloth: The cloth was purchased from Owens Corning fiberglas under the designation S/34-901. Governing specification was prepared by Brunswick to a specified weight (8.4-8.9 oz/yd) warp yarn (15-10/inch), fill yarn (45-49/inch), breaking strength (1050 lbs/in min), and ignition loss (1-29).

Resin system: The resin system was mixed from the following components:

Epon 828	100	Shell Chemical
Nadic Methyl Anhydride	80	Ciba (906)
Benzyldimethyl Amine	1	Maumee Chemical

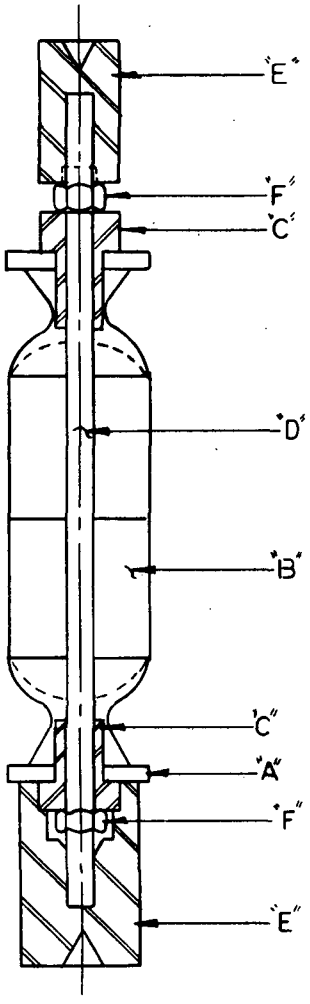

LEGEND

"A" Titanium Fitting

"B" Sand Mandrel

"C" Fitting - Wind Axis Adaptor

"D" Wind Axis

"E" Center Adaptors for Winders

"F" Lock Nut

Figure 5. Mandrel Assembly

The resin (Epon 828) was purchased to MIL-R-9300, Nadic Methyl Anhydride to WS 2359 Amend 1, and Benzyldimethyl Amine to WS 2357 Amend 1.

Titanium fittings: The fittings were machined from 5 AL.-2.5SN ELI conforming to MIL-T-9047D, Type II, Composition B.

Rod ends: The rod ends were purchased from Southwest Products Company, Monrovia, California as super alloy steel for cryogenic service. The rod ends were purchased to vendor specifications under SWRMS-4-100 SWRMLHS-4-100 SWRMS-6-100 and SWRMLHS-6-100 for various sizes, strengths and material characteristics.

Nut check: The material was corrosion-resistant steel to MIL-N-6034 to AN316C-6R, AN316C-6L, AN316C-8R, and AN316C-8L for size, tensile strength and thread size.

Radiation barrier: The barrier material composition was Dexter paper #X1303 (13.74 gms/M^2). These materials were chopped into flakes 1/4 to 1/2 inch square and mixed in the ratio of 88/12 (Dexter paper/mylar) by weight. The barrier was furnished by Hauser Research and Engineering Boulder, Colorado.

Filament winding - The assembled mandrel was placed in a helical winder and properly located for winding. A separator film (FEP) was placed over the exposed sand mandrel to prevent resin bonding to the mandrel surface.

The entire surface to be wound, including fittings, was coated with resin. The -1 and -3 tank supports were wound with one helical layer in accordance with Table VII. The ends were then wound using circumferential fibers and 143 fabric as shown in Figure 6. The fabric (2 plies) was extended down past the tangent line of dome and cylinder to provide a good shear bond between fabric and helical fibers during compression and tension loading. A final layer of circumferential fibers (Tabel VII) was then wound from fitting-to-fitting to complete the tank support wind.

The -2 tank support was similarly wound except the sequence was one helical layer followed by one circumferential fiber layer between dome/cylinder tangent liner, and then one additional helical layer in accordance with Table VII. The end build-up was performed in accordance with Figure 7. A final circumferential layer was wound between fittings to complete the winding.

All tank supports were then gelled at 52-66°C with heat lamps while rotating at 10-20 rpm. The final cure was in an air circulating oven at the cure schedule shown in Table VIII. The tank support struts were allowed to cool to <93°C before removal from the oven.

TABLE VII a - WIND SCHEDULE
(SI Units)

TANK SUPPORT CONFIGURATION			
	-1	-2	-3
Helical			
Band width, cm	.287/.299	.249/.262	.292/.305
Tension (wind), gms.	1134 ± 218	1134 ± 218	1134 ± 218
Wind angle, radians	.4854	.5311	.4854
No. layers	1	2	1
Circuits	36	47	36
No. rovings	3	2	3
Circs			
Rovings/inch (12 end)	6.69	10.03	6.69
No. rovings	3	2	3
No. plies	1	2	1
Wind tension, gm/12 end	1134 ± 218	1134 ± 218	1134 ± 218
Band width, cm.	.4064/.381	.2667/.254	.4064/.381
Materials			
Roving--S-901, 12-end glass, Resin: Epon 828/MNA/BDMA (100/90/.5/hr).			

NOTE: Roving preimpregnated by Brunswick Proprietary process to resin content of 23 ± 27.

TABLE VII b - WIND SCHEDULE
(Customary Units)

	TANK SUPPORT CONFIGURATION		
	-1	-2	-3
Helical			
Band width, in.	.113/.118	.098/.103	.115/.120
Tension (wind), lbs.	2½ ± ½	2½ ± ½	2½ ± ½
Wind angle, X°	27° 49"	30° 26"	27° 49"
No. Layers	1	2	1
Circuits	36	47	36
No. Rovings	3	2	3
Circs			
Rovings/inch (12 end)	6.69	10.03	6.69
No. rovings	3	2	3
No. plies	1	2	1
Wind tension, lbs/12 end	2½ ± ½	2½ ± ½	2½ ± ½
Band width	.160/.150	.105/.100	.160/.150
Materials			
Roving--S-901, 12-end glass, Resin: Epon 828/MNA/BDMA (100/90/.5/hr).			

NOTE: Roving preimpregnated by Brunswick proprietary process to resin content of 23 ± 27.

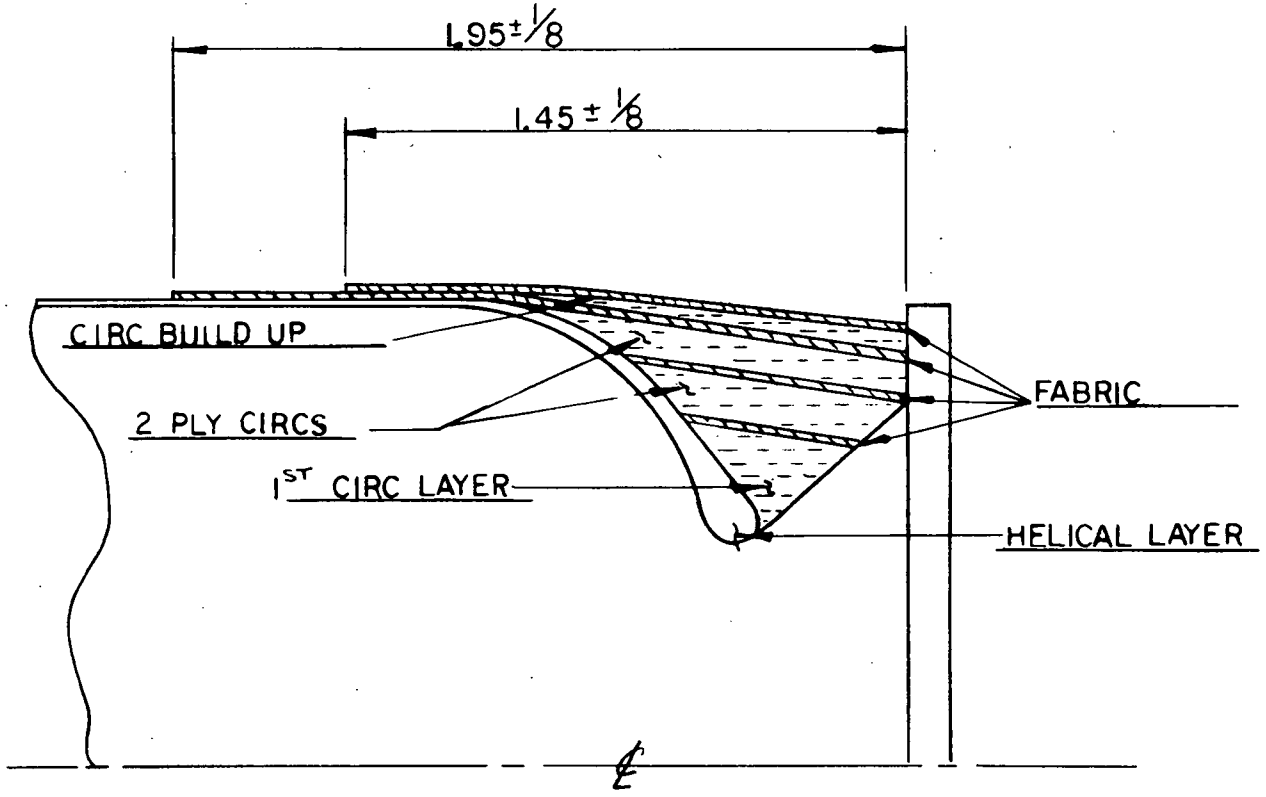

Figure 6. -1 and -3 Strut Joint Build-Up

TABLE VIII TANK SUPPORT CURE SCHEDULE

Time, Hrs.	Temperature, °C
2 ± 15 min.	100° ± 5.6°C
1 ± 10 min.	124.4° ± 5.6°C
1 ± 10 min.	148.9° ± 5.6°C

Final assembly - The wind axis was removed from the tank support and the water-soluable mandrel removed by injecting hot water (65.6°C) into the support. The support was then dried and inspected.

Radiation shield material was then placed inside the supports to a predetermined weight as shown in Table IX. The radiation barrier material was furnished by the Hauser Research and Engineering Company, Boulder, Colorado as part of their sub-contract on thermal radiation design. The radiation barrier material consisted of Dexiglass #X1303 (13.74 gm/M^2) and aluminized mylar .00025"t (9.12 gm/M^2) in a 87.54/12.46 ratio by weight.

TABLE IX RADIATION SHIELD

Tank Support	Weight/Support, gms
-1	22 gms
-2	19 gms
-3	10.2 gms

Spherical rod ends were then assembled to the supports using super alloy steel rod ends from Southwest Products, Monrovia, California. Standard AN316C jam nuts were used to lock the rod end to the support fittings within the prescribed length. Photographs of the completed support configurations are shown in Figures 2, 3 and 4.

Testing

Structural tests were conducted on five design verification units at both room and cryogenic temperatures and on nine production units at cryogenic temperatures. The test results are shown in Table X.

Room temperature test procedures - The room temperature tests were performed by the Brunswick Corporation in accordance with the following procedure:

TABLE Xa TEST RESULTS
(SI Units)

Serial No.	Dash No.	Test	Temp. (°C) Cold End	Center	Warm End	Bore-Bore Length (cm)	Load at Failure (Newtons)	Spec. Req. on Load (Newtons)	Resulting Margin of Safety	Min.** Calc. Margin	Cylinder Wall Stress (N/CM^2)	Remarks
01X-1	-1	Comp.	Rm	Rm	Rm	65.79	- 8,006	- 5,560	0.44	Crip. 2.96 Col. .78	- 8,961	Column buckling at center of cylinder.
005	-1	Comp.	-241	-217	-86	66.47	-18,415	- 5,560	2.31	Crip. 2.96 Col. .74	-20,610	Column buckling or compressive crippling at center of cylinder.
001	-1	Comp.	-219	-222	-60	66.47	-19,082	- 5,560	2.43	Crip. 2.96 Col. .74	-21,357	Column buckling or compressive crippling at center of cylinder.
006	-1	Tens.	-242	-230	-90	66.47	+13,220	+ 6,761	7.70	Stress 8.52	+65,811	Stress failure near joint in cylinder near warm end.
01X-2	-2	Comp.	Rm	Rm	Rm	46.68	-47,149	-25,087	0.88	Col. .80 Crip. 1.41	-27,408	Column buckling at center of cylinder.
04X-2	-2	Comp.	-192	- 5	-60	47.96	-13,150	-25,087	1.31	Col. .71 Crip. 1.41	-34,001	Column buckling or compressive crippling at center of cylinder.
013	-2	Comp.	-187	- 33	-41	47.96	-71,168	-25,087	1.84	Col. .71 Crip. 1.41	-41,370	Column buckling or compressive crippling at center of cylinder.
015	-2	Comp.	-190	- 32	-51	47.96	-56,490	-25,087	1.25	Col. .71 Crip. 1.41	-32,837	Column buckling or compressive crippling at center of cylinder.
02X-2	-2	Tens.	Rm	Rm	Rm	47.96	+87,403	+36,918	1.37	Stress 2.94	+50,807	Stress failure in cylinder near joint, (joint reinforcement fwd of fitting where failure occurred was partly sanded through).
03X-2	-2	Tens.	-190	- 32	-40	47.96	+100,524	+36,918	1.73	Stress 2.94	+58,435	Dowel pin failure.
014	-2	Tens.	-190	- 43	-51	47.96	+91,184	+36,918	1.47	Stress 2.94	+53,005	Compressive crippling at midpoint of cylinder.
.001	-3	Comp.	-187	- 48	-59	35.31	-25,620	- 8,318	2.09	Col. 3.35 Crip. 1.74	-28,674	Compressive crippling at midpoint of cylinder.
011	-3	Comp.	-185	- 60	-52	35.31	-33,600	- 8,318	3.01	Col. 3.35 Crip. 1.74	-37,336	Compressive crippling at 1/4 point of cylinder near warm end.
002	-3	Tens.	-187	- 43	-52	35.31	+54,444	+ 9,919	4.49	Stress 6.63	+60,933	Stress failure near joint in cylinder at cold end.

*Design verification units
**Crip. stands for local compression crippling
Col. stands for column buckling

TABLE Xb TEST RESULTS

(Customary Units)

Serial No.	Dash No.	Test	Temperature (°F) Cold End	Center	Warm End	Bore-Bore Length (in)	Load at Failure (lb)	Spec. Req. on Load (lb)	Resulting Test Margin of Safety	Min.** Calc. Margin	Cylinder Wall Stress (psi)	Remarks
01X-1*	-1	Comp.	Rm	Rm	Rm	25.90	-1,800	-1,250	0.44	Crip. 2.96 Col. .78	-12,996	Column buckling at center of cylinder.
005	-1	Comp.	-402	-358	-123	26.17	-4,140	-1,250	2.31	Crip. 2.96 Col. .74	-29,891	Column buckling or compressive crippling at center of cylinder.
001	-1	Comp.	-361	-368	-77	26.17	-4,290	-1,250	2.43	Crip. 2.96 Col. .74	-30,974	Column buckling or compressive crippling at center of cylinder.
006	-1	Tens.	-404	-383	-129	26.17	+13,220	+1,520	7.70	Stress 8.52	+95,448	Stress failure near joint in cylinder near warm end.
01X-2*	-2	Comp.	Rm	Rm	Rm	18.38	-10,600	-5,640	0.88	Col. .80 Crip. 1.41	-39,750	Column buckling at center of cylinder.
04X-2*	-2	Comp.	-313	+23	-77	18.88	-13,150	-5,640	1.31	Col. .71 Crip. 1.41	-49,312	Column buckling or compressive crippling at center of cylinder.
013	-2	Comp.	-305	-28	-41	18.88	-16,000	-5,640	1.84	Col. .71 Crip. 1.41	-60,000	Column buckling or compressive crippling at center of cylinder.
015	-2	Comp.	-310	-25	-60	18.88	-12,700	-5,640	1.25	Col. .71 Crip. 1.41	-47,625	Column buckling or compressive crippling at center of cylinder.
02X-2*	-2	Tens.	Rm	Rm	Rm	18.88	+19,650	+8,300	1.37	Stress 2.94	73,687	Stress failure in cylinder near joint, (joint reinforcement fwd of fitting where failure occurred was partly sanded through).
03X-2*	-2	Tens.	-309	-25	-40	18.88	+22,600	+8,300	1.73	Stress 2.94	84,750	Dowel pin failure.
014	-2	Tens.	-310	-46	-60	18.88	+20,500	+8,300	1.47	Stress 2.94	76,875	Stress failure in cylinder near joint at warm end.
.001	-3	Comp.	-305	-55	-75	13.90	-5,760	-1,870	2.09	Col. 3.35 Crip. 1.74	-41,587	Compressive crippling at midpoint of cylinder.
011	-3	Comp.	-301	-77	-63	13.90	-7,500	-1,870	3.01	Col. 3.35 Crip. 1.74	-54,150	Compressive crippling at 1/4 point of cylinder near warm end.
002	-3	Tens.	-305	-45	-62	13.90	+12,240	+2,230	4.49	Stress 6.63	+88,373	Stress failure near joint in cylinder at cold end.

*Design verification units

**Crip. stands for local compression crippling
Col. stands for column buckling

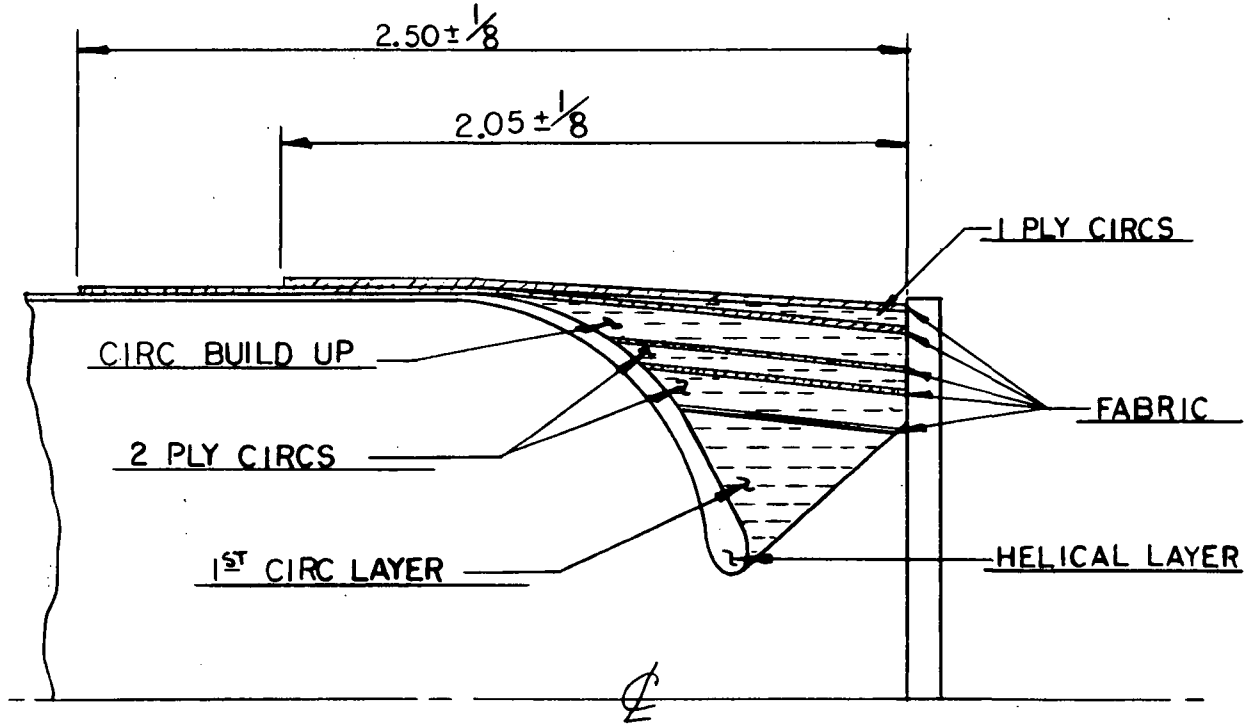

Figure 7. -2 Strut Joint Build-Up

1.0 EQUIPMENT

Brunswick Drawing TF-083670, Details 1 and 2 for -1 and -3 configurations (clevis and pin)
Brunswick Drawing TF-083670, Details 3 and 4 for -2 configuration (clevis and pin)
222,400 Newtons (50,000 lb.) minimum tension-compression machine

2.0 TEST PROCEDURE

Table XI lists the three parts to be tested along with the bore-bore length setting and load rate.

TABLE XI STRUT TEST LENGTH AND LOAD RATE

	Bore-Bore Length		Load Rate	
	cm	(in)	Newton/min	(lb/min)
BLD 836701-1	66.47	26.17	4448	1000
BLD 836701-2	47.96	18.88	88.96	2000
BLD 836701-3	35.31	13.90	4448	1000

1) Adjust length in accordance with Table XI.
2) Set-up room temperature compression test in accordance with Figure 8.
3) Apply load at rate specified in Table XI until failure occurs.
4) Set-up for tensile test in accordance with Figure 8.
5) Apply load at rate specified in Table XI until failure occurs.

Cryogenic test procedure - The structural testing at cryogenic temperatures was performed by the Hauser Research and Engineering Company, Boulder, Colorado in accordance with the following procedure:

1.0 EQUIPMENT

1. Tensile/Compression Test Machine - 111,200 newtons (25000 lb) capacity.
2. Data Recorder - 10 channels min.
3. Liquid Helium.
4. Liquid Nitrogen.
5. Gaseous Helium.

2.0 APPLICABLE DOCUMENTS

1. NASA Spec. C-305892 - Specification for filament-wound fiberglass supports
2. Drawing BLD 836702 space support, cryogenic tank.

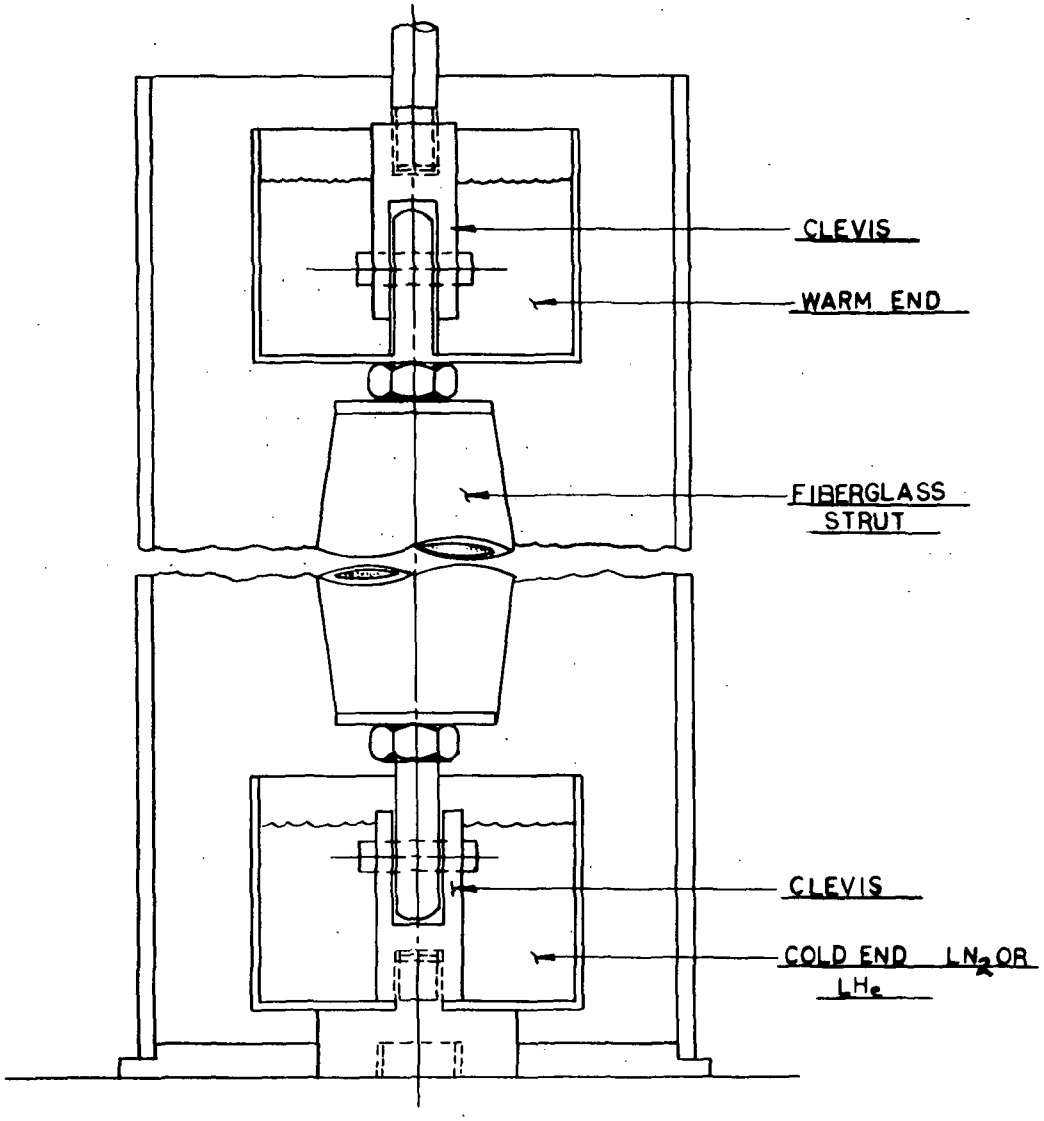

Figure 8. Test Set-Up

3.0 TEST PROCEDURE

A total of seven copper-constantan thermocouples were installed on each support at the locations specified in Figure 9. Narmco #3170/7133 adhesive or equivalent was used with one exception. During the -1 test, a gold-iron-chromel P Thermocouple was used on the fitting at the cold end. Four uniaxial strain gages were installed on each support at the locations shown on Figure 9. Gages were micro-measurements #SK-09-250BP-120 or equivalent.

The rod ends were adjusted to the following dimensions:

-1 configuration = 66.47 cm (26.17")

-2 configuration = 47.96 cm (18.88")

-3 configuration = 35.31 cm (13.90")

The struts were then cooled down to a stabilized temperature using LN_2 for the -1 strut and dry ice for the -2 and -3 struts.

After initial stabilization, the cryostat covers were removed and a mixture of 1-hexanol or chlorobenzene and LN_2 was installed in the upper coolant cup. This partially frozen mixture held the metal end fitting of the strut at a temperature of about -51°C (-60°F).

The cryostat cover was replaced and a helium flush was started through the cryostat. Coolant was added to the lower cup (Figure 9) until the level reached the interface between the lower fitting and lock nut. This level was maintained within +0-1 inch during test. The coolant used was liquid helium LHe for -1 configuration and LN_2 for -2 and -3 configuration tests. Temperature was -253°C (-423°F) -1 configuration and -196°C (-320°F) for the -2 and -3 configurations.

Upon reaching equilibrium, each strut was loaded at a rate of .254 cm/min (0.10 inches/min.) for crosshead travel. The loading direction was as follows:

-1 configuration: 1 strut in tension, 2 in compression

-2 configuration: 1 strut in tension, 2 in compression

-3 configuration: 1 strut in tension, 2 in compression

Loading continued until each strut failed. Strain measurements and crosshead travel were continuously recorded. Temperature was recorded several times during the loading and immediately after failure.

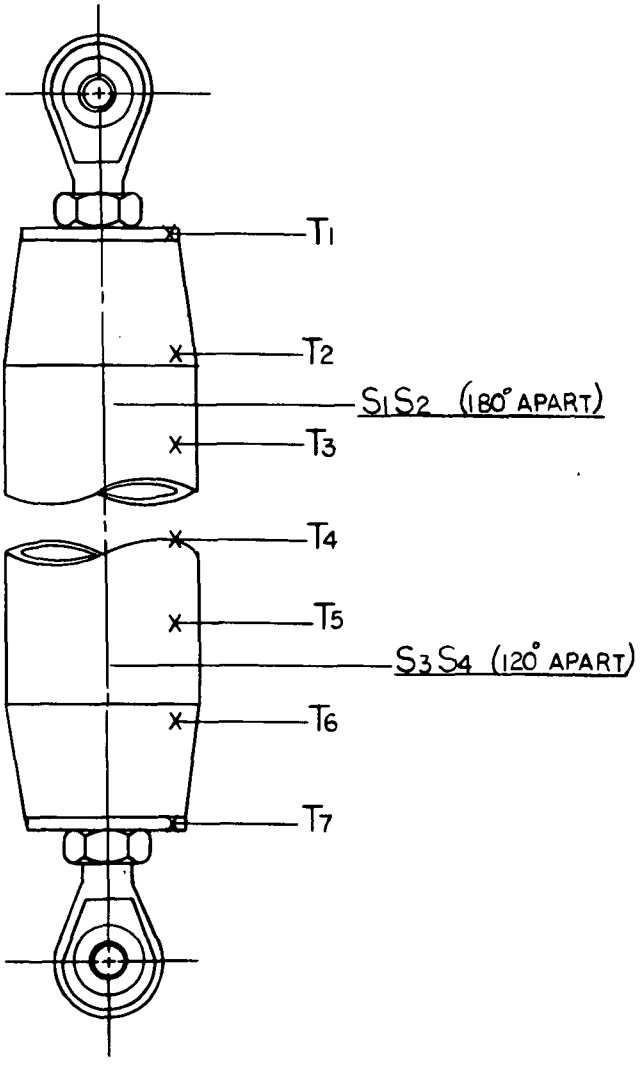

LEGEND

T = THERMOCOUPLE

S = STRAIN GAGE

Figure 9. Thermocouple and Strain Gage Location

4.0 DISCUSSION OF TEST RESULTS

No design changes were made after the design verification tests; therefore, the entire group of results can be discussed collectively. The compression test results will be discussed first.

Compression test results:

-1 Strut. A total of three -1 struts were tested in compression; one design verification unit at room temperature and two production units at cryogenic temperatures.

As can be seen in Table X, all three units exceeded the ultimate design load requirement of 5560 Newtons (1250 lbs.). The room temperature strut failed at 8006 Newtons (1800 lbs.) in column buckling. The actual failure load was below the predicted value. The two at cryogenic temperature failed in either column buckling or compression crippling at a value which greatly exceeded the predicted value for column buckling 18,415 Newtons (4140 lbs.) and 19,082 Newtons (4290 lbs.). The predicted margin on column buckling was based on the actual length of the test specimen and the room temperature 24°C (+75°F) modulus values. The lower room temperature result can be explained as normal scatter for a column buckling failure.

The marked increase in cryogenic test results cannot be explained by the 11% increase in modulus at the lower temperatures of -222°C (-368°F) and -230°C (-383°F) at the center of the strut. The strength and modulus variation as a function of temperature is plotted in Figure 10. This data is based on NOL ring data obtained from the following NASA publication:

> Morris, E. E.; Darms, F. J.; Landes, R. E.; and Campbell, J. W.: Parametric Study of Glass-Filament-Reinforced Metal Pressure Vessels. NASA CR 54-855, April 1966.

The most logical explanation is that the ball swivel joint did not act as a frictionless pinned end. This would increase the resistance to column buckling. There was no lubricant on the ball joint or the fixture because none is permitted in the actual application. In a previous program, Brunswick experienced a difference of 2 to 2.5 times between column buckling test results conducted with lubricated pins and non-lubricated pins.

The explanation and conclusions made on the -1 strut are applicable to the -2 struts.

-2 Strut. Four -2 struts were tested in compression: One design verification unit at room temperature and one at cryogenic temperature; and two production units at cryogenic temperature. All four struts exceeded the required load of 25,087 Newtons (5640 lbs.).

The room temperature unit failed at slightly above the predicted value. A photograph of this unit is shown in Figure 11.

The failure of the three struts at cryogenic temperature was similar to the -1 strut failure in that: (1) they failed higher than predicted for column buckling which could be explained by a modulus increase (in this case less than 3% at temperatures between -33°C (-28°F) and -51°C (-60°F) at the center; (2) they approached the predicted crippling value in two cases and exceeded it in one case; (3) the values were reasonably close, ranging from 56,490 Newtons (12,700 lbs.) to 71,168 Newtons (16,000 lbs.).

-3 Struts. Two -3 production units were tested in compression at cryogenic temperatures. The struts failed at loads of 25,620 Newtons (5760 lbs.) and 33,600 Newtons (7500 lbs.). Both units failed in compression crippling, one at the midpoint and one at the quarter point near the warm end. This can be stated definitely because both units exceeded the predicted value for column buckling. The appearance of the failure was similar to the failure of all the other compression failures.

Tensile test results:

A total of five struts were tested in tension. Two design verification tests were performed on the -2 strut, one each at room and cryogenic temperatures. One production unit of each configuration was tested at cryogenic temperatures. While all three strut configurations greatly exceeded the tensile load requirement, none reached the predicted cylinder room temperature wall stress of 86,877 N/cm^2 (126,000 psi). All struts except S/N 03X-2, which failed the dowel pin, failed in the cylinder section at about 3.81 to 7.62 cm (1.5 to 3.0 inches) from the joint. Three failed near the warm end joint and one failed near the cold end. A photograph of the failed -1 S/N 006 strut is shown in Figure 12 and a photograph of the failed -2 S/N 02X-2 strut is shown in Figure 13. Very little crazing was evident in the failed units outside of the immediate failure area.

The average tensile stress in the fiberglass cylinder, due to the maximum load during the cryogenic test, is listed in Table XII, under the heading "Test Result Stress". For the purpose of comparing the test result stress with the predicted failure stress calculated at room temperature), the test result stress has been converted to an "Equivalent Room Temperature Stress" in Table XII. The curve in Figure 10 was used to calculate the equivalent room temperature stresses. Failure was assumed to occur at the warmest point in the strut.

In reviewing the test results, it is seen that the attained stress values were approximately 60-65% of the predicted value. There was very little scatter in the results, with the -1 and -3 struts attainind a slightly higher value than the -2 struts. This is somewhat reasonable since the helical wind angle was slightly less (a lower

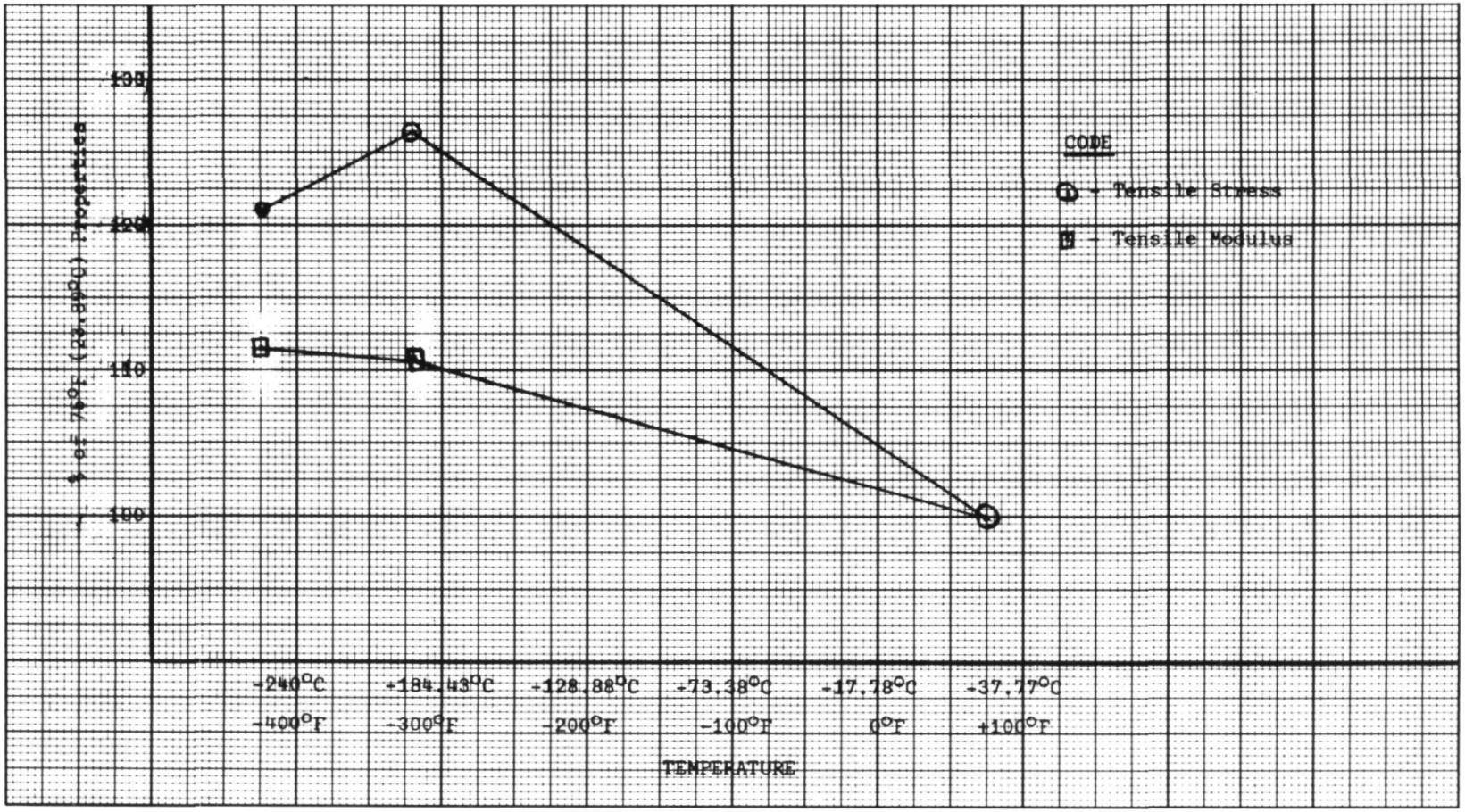

Figure 10. Tensile Stress and Modulus vs Temperature

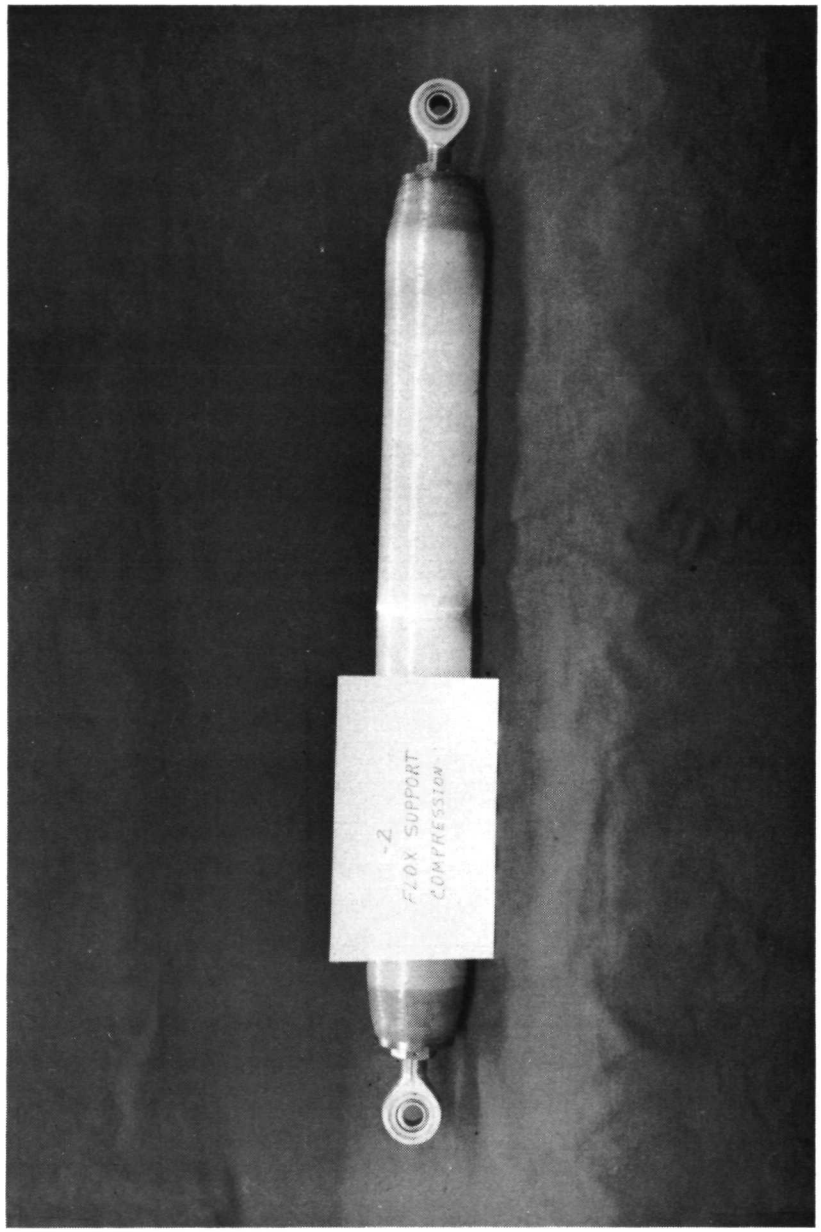

Figure 11. -2 Strut Compression Failure

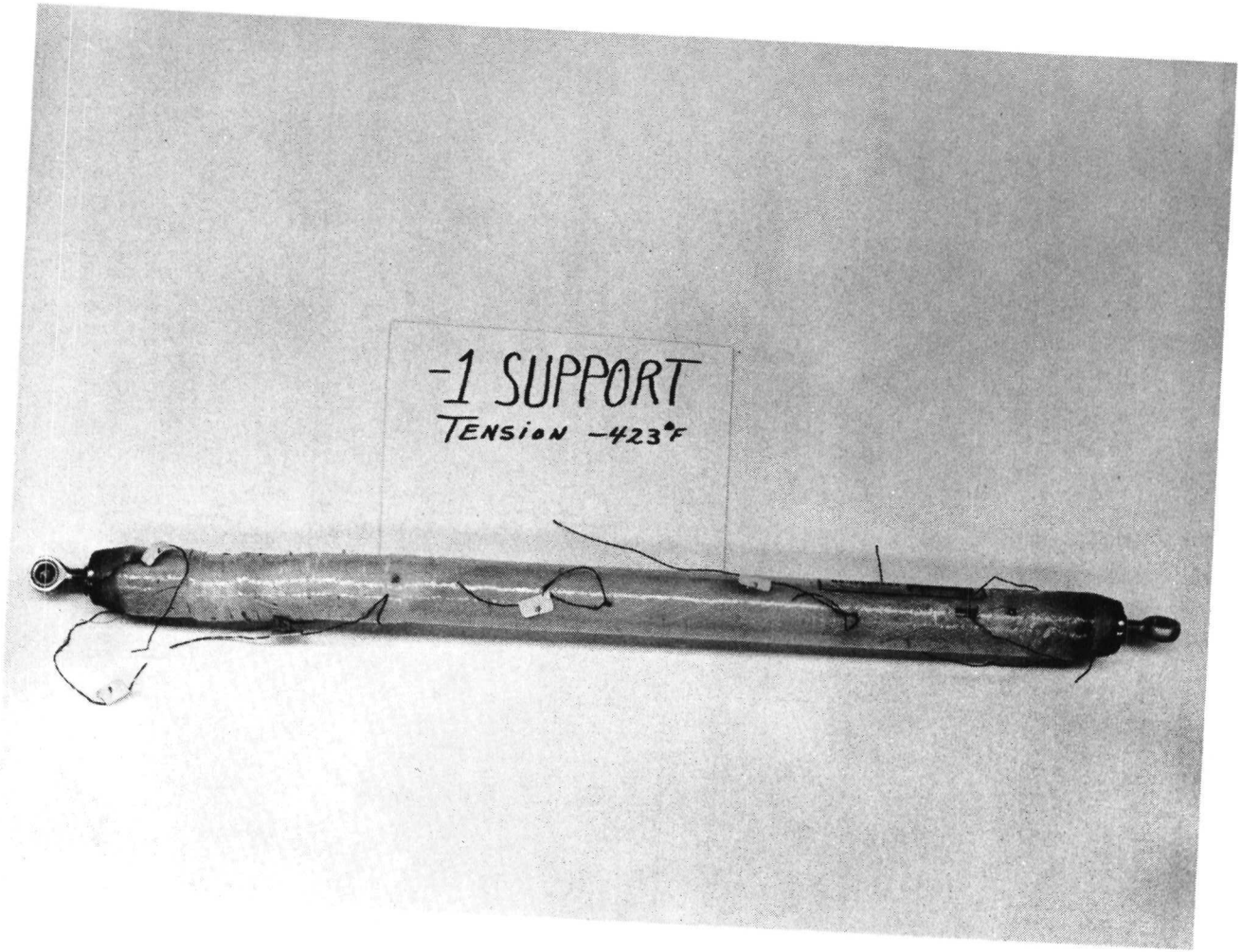

Figure 12. -1 Strut Tension Failure

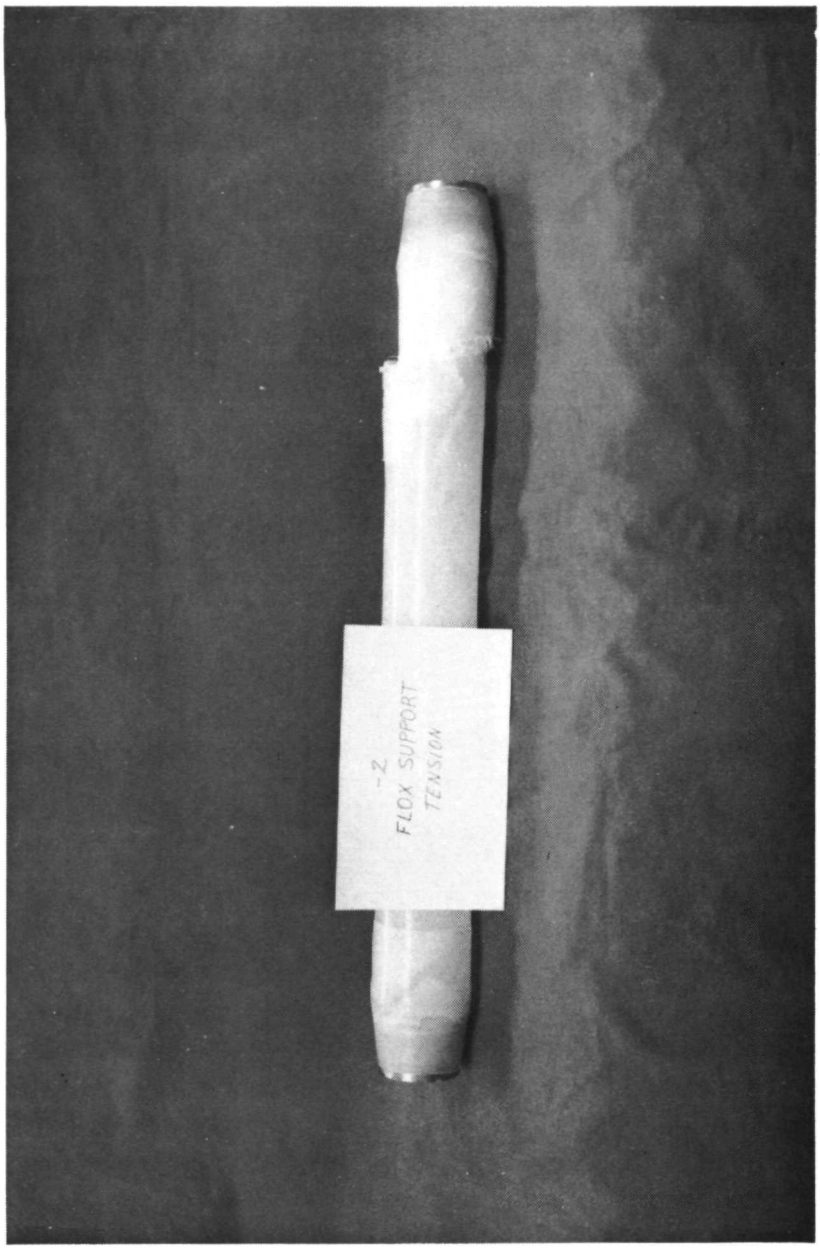

Figure 13. -2 Strut Tension Failure

TABLE XII TENSILE TEST RESULTS

Dash No.	S/N	Test Result Stress		Warmest Temperature		Allowable Stress Increase %	Equivalent Room Temperature Stress	
		N/cm^2	(psi)	°C	°F		N/cm^2	(psi)
-1	.006	65,811	95,448	-89.4	-129	13	58,240	84,467
-2	02X-2	50,807	73,687	+23.9	+ 75	0	50,807	73,687
-2	03X-2	58,435	84,750	-31.7	- 25	6.5	54,868	79,577
-2	.014	53,005	76,875	-43.3	- 46	7	49,537	71,845
-2	.002	60,933	88,373	-42.8	-45	7	56,946	82,591

wind angle results in a higher longitudinal strength) in the -1 and -3 and the ratio of helicals to hoops was 2.6 versus 2.04 for the -2. This advantage in theoretical longitudinal strength is partially reduced by the fact that the -1 and -3 struts have a thinner, one sequence (one helical layer and 1 hoop ply wall) construction. In the -1 and -3 units, the fiber in the helical layer and 1 hoop ply wall) construction. In the -1 and -3 units, the fiber in the helical layer did not actually break but merely pulled away from the hoop ply. This is seen in the photograph in Figure 12.

Following are two possible explanations as to why the tensile failures were less than the predicted value:

1) Since all the failures occurred near the joint at the end of the cloth reinforcement, it is possible that the load redistribution at this point had something to do with the less-than-predicted test failure. Perhaps the local reinforcement at the joint should extend out further and have a more gradual taper.

2) This type of wind pattern depends upon shear transfer between layers for developing uniaxial strength. In a many-layer construction almost all helical layers will be reinforced on both sides. In a one-sequence design, like the -1 and -3 struts, only one side of the helical is reinforced by circumferential windings, while in the two-sequence -2 struts, 50% of the load is in a helical layer that has only one side reinforced with circumferential windings. The type of failure shown in Figure 13, where the inner helicals pulled away from the outer circumferential windings, offers some justification for this reasoning.

Proof load test at room temperature:

Each tank support underwent a proof load compression and tensile test, at room temperature, prior to delivery to NASA. The compression and tensile proof loads were about 25% less than the ultimate compression and ultimate tensile design loads respectively. The loads were applied in a Baldwin-Southwark testing machine. Load and crosshead travel were recorded in increments up to the proof load for each support. All supports passed the proof load test with no evidence of structural degradation.

CONCLUSION

The filament wound fiberglass tank support design employed in this program has proven to be a reliable and efficient structure which is lightweight and provides low thermal conductance and economical production with standard filament winding equipment for cryogenic service to 37°R (20.55°K). The most significant contribution to the design effort was the joint design which yielded joints as strong as the cylinder wall with reproducible structural performance. This was achieved through an integrated fiberglass structure which does not rely on secondary and primary adhesive bonds for end fitting attachment.

A tool package and fabrication procedure was developed which provides reliable, reproducible and economical production of tank supports in large or small production quantities.

APPENDIX A

THERMAL ANALYSIS
OF
CRYOGENIC STRUTS

prepared for

THE BRUNSWICK CORPORATION

by

Hauser Research and Engineering Co.

Boulder, Colorado

Report No. 5274-70-16

Copy No. _____

THERMAL ANALYSIS OF CRYOGENIC STRUTS

A special study for Brunswick Corporation,
Defense Products Division, Lincoln, Nebraska
Mr. J. S. Carter, Product Engineering Manager

P. O. #DN 10-0201, Task 1

for contract NAS3-14627

Report prepared and submitted by:

Ray L. Hauser

Dr. Ray L. Hauser, Research Director

CONTENTS

TABLES

FIGURES

THERMAL ANALYSIS OF CRYOGENIC STRUTS

1. INTRODUCTION

The objective of this study was to identify thermal conductivity values for glass/epoxy composite materials and to predict heat transfers and temperature gradients in cryogenic struts.

The -1 strut for use with liquid hydrogen tanks was to be analyzed for heat conduction and internal radiation in a vacuum, coast condition. This strut was also to be analyzed for heat conduction and convection in a helium atmosphere.

The -2 strut for use with flox tanks and the -3 strut for use with liquid methane were to be analyzed for heat conduction and convection in a helium atmosphere.

The struts of this study are described by Brunswick Drawing # BLD 836701.

2. MATERIALS PROPERTIES

Prior government-funded studies have provided sufficient background of data regarding the thermal conductivities of materials concerned for this application.

The thermal conductivity of titanium has been reported by Hust and Powell (Ref. 1) throughout the cryogenic temperature range of concern in this study. Their graphical data for A-110AT alloy (5% AL, 2.5% SN) have been transcribed as follows:

Table 1 - Thermal Conductivity of Titanium A-110AT (Ref. 1)

Temperature ^{o}R.	Conductivity, Btu ft/hr ft^{2} ^{o}F.
10.8	0.318
18	0.565
36	1.10
72	1.82
108	2.19
144	2.48
180	2.77
270	3.29
360	3.81
540	4.62

Two sources were found for primary data on thermal conductivity of glass at cryogenic temperatures. Stevens (Ref. 2) studied Pyrex glass over the temperature range of 165 to 590^{o}R and used relatively small temperature increments between warm and cold sides of each specimen. White (Ref. 3) studied conductivity into the hydrogen/helium range using standard cryogens for his warm and cold side conditions. Both sources of data fit second-order polynomial curves, but there is a considerable discrepancy between their reported and extrapolated values noted in Table 2 and Figure 1. These differences range from 0.5% at 500^{o}R. to 35% at 150^{o}R. and may be due to different Pyrex glass formulas or to technical errors.

Glass conductivity is approximately 10% that of titanium. Thermal conductivity data on glass/epoxy composites are available from three sources that have been used in prior studies of cryogenic struts. The laminate tests of an Arthur D. Little (ADL) report (Ref. 4), laminate tests from Hertz and Haskins at General Dynamics Astronantics (GDA) (Ref. 5), and strut conduction tests performed by Lockheed (Ref. 6) are pertinent.

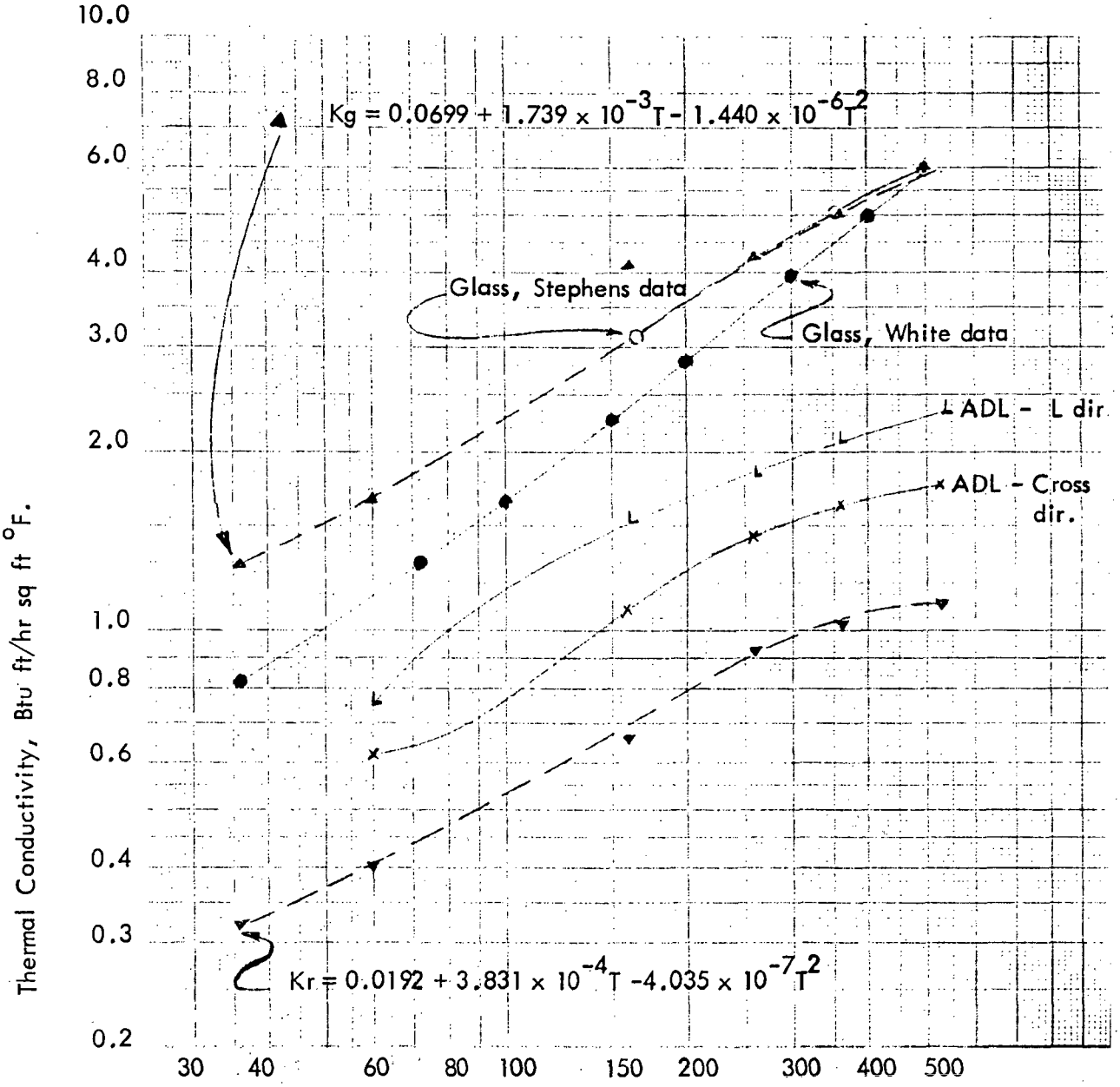

Figure 1. Thermal Conductivity of Glass, ADL Laminate (Ref. 4) and Resin

Table 2 - Thermal Conductivity of Pyrex Glass

Temperature °R			Conductivity, Btu ft/hr ft^2 °F.	
T_1	T_2	Tave or calc*	Stephens (Ref. 2)	White (Ref. 3)
36	7.2			.063
138.6	7.2			.132
138.6	36.0			.147
		36*		.0826
		72*		.1296
		100*		.1652
		150*		.2269
		165.5	0.312	
		200*		0.286
		300*		0.397
		352	0.508	
		357	0.515	
		400*		0.499
		495	0.593	
		500*		0.590
		504	0.595	
		590	0.634	
540	7.2			0.358
540	36.0			0.374
540	138.6			0.431

* White data fit the equation $K = 3.444 \times 10^{-2} + 1.357 \times 10^{-3}T - 4.912 \times 10^{-7}T^2$

In all three of these references, the geometry and content of glass and epoxy resin were described. The ADL data were based upon a NEMA G-10 laminate containing 64% of style 1674 glass fabric and 36% weight of an amine-cured epoxy. The GDA data reported here were from samples D-1 and D-2 containing 26.47 and 36.57% resin, respectively. Resin was DER 332 cured with MNA and DMP-30. The glass was unidirectional in both samples and was described as YM-31A high modulus glass containing beryllia. Haskins and Hertz reported different conductivities in atmospheres of nitrogen and helium; the former are listed in Table 3. The Lockheed data were based upon a strut having eight longo layers and three circ layers of glass. The glass was S-901 and the resin was Epon 828

cured with 90 pbw MNA and 0.55 pbw BDMA, with 20.5% resin, 79.5% glass. Conductivity of the strut was reported by Lockheed to fit the curve, $K = 0.050 + 6.35 \times 10^{-4} T$. The three references are compared using consistent units in Table 3 and Figure 2.

Table 3 - Thermal Conductivity of Glass - Epoxy Composites

Kc = across filaments
Kl = along filaments

Temperature °R	Conductivity				
	ADL Kc (4)	ADL Kl (4)	GDA Kc (5)	GDA Kl (5)	Lockheed(6)
40			0.083	0.139	0.075
60	0.062	0.075			0.088
140			0.117	0.174	0.140
160	0.108	0.154			0.152
260	0.146	0.183	0.142	0.210	0.216
360	0.162	0.208	0.157	0.236	0.278
460					0.342
510			0.180	0.256	0.373
528	0.175	0.233			0.386

At temperatures mid-range of Table 3 the data appear to be fairly consistent. Conductivity across filaments appear to be about the same for ADL and GDA laminates. Conductivity along the filaments is again similar, except that the GDA values are about 10% higher. The Lockheed struts had mostly filaments in the direction of heat flow and were quite similar to GDA data at 260°R.

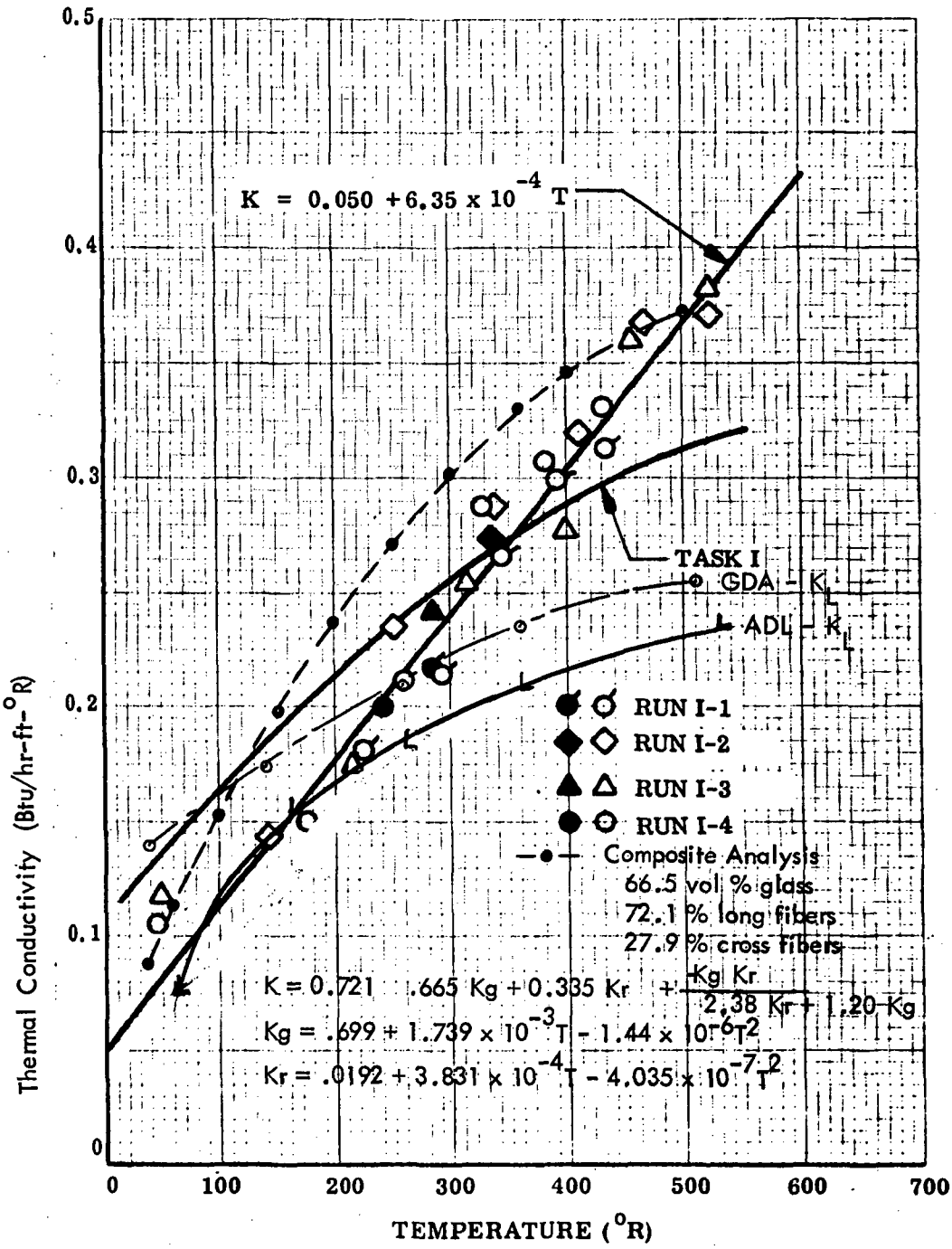

Figure 2. Thermal Conductivity of Lockheed Strut (Ref. 6)
GDA (5) and ADL Laminates (4) and Composite Analysis of Lockheed Strut

Two significant features of these data must be noted that influence their acceptability. The GDA study used glass with high beryllia content; beryllia has a thermal conductivity about 10 times that of E-glass or S-glass. The Lockheed strut data were based upon an assumption that conduction was the only mode of heat transfer; unless the Dexiglass used to fill the struts had been metallized or foil-laminated (unreported), the radiation heat transfer was partly diffused, partly opacified. Radiation transfer within the strut would cause apparent low conductivity at the cold end and apparent high conductivity at the warm end.

The ADL data have been accepted as presenting the most reliable basis available for analyzing the thermal conductivity of glass/epoxy composite in the cryogenic temperature range.

A simple model has been prepared to delineate the conductive factors of the glass and resin phases of glass/epoxy composites. This model assumes rectangular-shaped glass filaments stacked in a resin matrix with glass conduction in parallel or resistances in series depending upon whether heat is flowing along or across the filaments. The following sketch and calculations represent this model for the ADL laminate (Ref. 4).

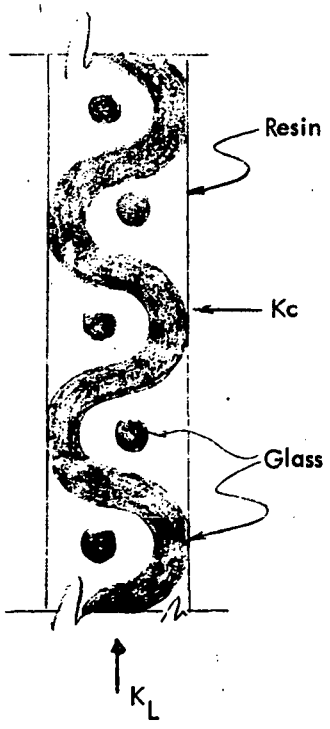

Wg = wt. fraction glass = 0.64
Vg = vol. fraction glass =
$Wg\,\rho g / Wg\,\rho g + (1 - Wg)\,\rho r$
ρg = density of glass = 2.54
ρr = density of resin = 1.30

1. $\frac{Lc}{Kc\ Ac} = \frac{Lg}{Kg\ Ag} + \frac{Lr}{Kr\ Ar}$

Resin and glass layers in series.

2. $Kc = \frac{Kg\ Kr}{0.476\ Kr + .534\ Kg}$

3. $\frac{Kl\ A}{L} = \frac{kg\ Ag}{Lg} + \frac{kr\ Ar}{L} + \frac{kc\ A}{L}$

$$Lg = 1.10\ L$$
$$Ag/A = \frac{0.50\ vg}{1.10} = 0.216$$
$$Ar/A = 0.5\ (1-vg) = 0.267$$

4. $Kl = 0.5\ Kc + 0.197\ Kg + 0.267\ Kr$

5. $Kg^2 + (2.78\ Kc - 5.06\ Kl)\ kg + 2.41\ Kl\ Kc - 1.205\ Kc^2 = 0$

6. $Kr = 3.74\ Kl - 1.87\ Kc - 0.739\ Kg$

Equations 1 and 3 describe the cross conductivity and the lengthwise conductivity as related to the glass or resin phase material and dimensions. By solving simultaneously equations 2 and 4, the thermal conductivity of glass may be obtained explicitly in the quadratic equation 5 from measured values K_c and K_L. Then the thermal conductivity of the resin may be obtained by equation 6.

The ADL data were analyzed by these equations, and the values of each phase conductivity are as noted in Table 4.

Table 4 - Thermal Conductivity of Glass and Resin in ADL Laminate as Calculated from Composite Analysis

Temperature °R.	Conductivity, Btu fr/hr ft^2 °F.	
	Glass, Kg	Resin, Kr
60	0.168	0.0404
160	0.416	0.0662
260	0.430	0.0935
360	0.504	0.1028
528	0.588	0.1095

With the exception of Kg at 160°R., these values are consistent with glass data of Stephens and are consistent with reported values for thermal conductivity of epoxy resins near 528°R. Equations representing these data are:

7. $Kg = 0.0699 + 1.739 \times 10^{-3}T - 1.440 \times 10^{-6}T^2$

8. $Kr = 0.0192 + 3.831 \times 10^{-4}T - 4.035 \times 10^{-7}T^2$

Recalculation of Kc and K_L from equations 7, 8, 2 and 4 has indicated values within 2% those reported by ADL except for the K_L at 160°R where the difference was 15% higher measured conductivity.

Equations 7 and 8 have been presented on Figure 1 for comparison with reported data on glass and composites. These equations provide the basis for subsequent analysis of thermal conductivity of struts described by Brunswick Drawing #BLD 836701. These equations are considered to have a precision of ± 20% if the ADL data have a precision of ± 10%.

The glass and resin data have also been analyzed in the Lockheed strut composite and results are shown in Figure 2. Close agreement is noted at the extremes, but the analysis is 20-35% conservative at the mid-range temperatures.

3. COAST ENVIRONMENT OF THE LIQUID HYDROGEN STRUT

The analysis for the -1 liquid hydrogen strut is based upon assumptions of zero convection and zero external radiation.

3.1 CONDUCTION

The composite geometry of the -1 liquid hydrogen strut is as follows for filament winding containing 80% glass by weight:

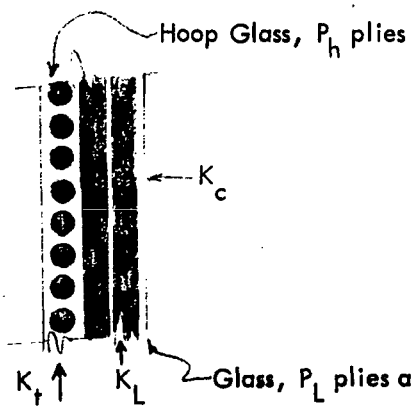

Wg = wt. fraction glass = 0.80

Vg = vol. fraction glass = $\frac{Wg\ \rho g}{(Wg\ \rho g + (1 - Wg)\ \rho r}$

ρg = density of glass = 2.54

ρr = density of resin = 1.3

$P_L = 2$ $P_H = 1$ A = .000962 sq. ft.

$L_o = 21.77 = 1.812$ Ft.

The thermal conductivities of struts may be described in general terms as in the previous composite analysis.

9. $$\frac{K_L A}{L} = \frac{Kg\ Ag}{Lg} + \frac{Kr\ Ar}{Lr} + \frac{Kt\ At}{L}$$

$$Ag/A = Vg \frac{P_L}{P_L + P_H} \cos \Theta \qquad \Theta = \text{Wind Angle}$$

$$Lg = L \sec \Theta$$
$$Lr = L \sec \Theta$$
$$Ar = (1-Vg) \frac{P_L}{P_L + P_H}$$
$$Ac/A = \frac{P_H}{P_L + P_H}$$

10. $$Kc = \frac{Vg}{kg} + \frac{1-Vg}{kr}$$

11. $$\frac{Q_L L_o}{A T} = -Kg\ Vg \frac{P_L}{P_L P_H} \cos^2 \Theta - Kr\ Vr \frac{P_L}{P_L P_H} \cos^2 \Theta$$

$$\frac{-P_H\ Kg\ kr}{(P_L + P_H)\ (Vg\ kr + (1-Vg)kg)}$$

12. Where $kg = kog + AgT + Bg\ T^2$

13. $kr = kor + Ar\ T + Br\ T^2$

14 $$\frac{Q_L L_o}{A} = -\int_{T_1}^{T_2} Vg \frac{P_L}{P_L + P_H} \cos^2 \Theta\ (kog + AgT + Bg\ T^2)\ dT$$

$$- \int_{T_1}^{T_2} Vr \frac{P_c}{P_L + P_H} \cos^2 \Theta\ (kor + Ar\ T + Br\ T^2)\ dT$$

Equation continued on following page.

$$- \int_{T_1}^{T_2} \frac{P_L}{(P_L + P_H)} \frac{(kog + Ag\,T + Bg\,T^2)\,(kor + Ar\,T + Br\,T^2)\,dT}{vg\,(kor + Ar\,T + Br\,T^2) + (1-Vg)\,(kog + Ag\,T + Bg\,T^2)}$$

15. $$Kc = \frac{Kg\,Kr}{vg\,Kr + (1-vg)kg}$$

Substitiution of the glass and resin conductivities (Eqns. 7&8) in the integration of Eqn. 14 permits calculation of the total conductive heat transfer in the axial direction of the hydrogen strut. This has been accomplished using an L_o of 1.81 ft. and a cross-section area of 9.62×10^{-4} sq. ft.

Total linear conduction for the hydrogen strut with 520 and 37°R. temperatures at the cylindrical section boundaries is thus calculated to be .0566 Btu/hour. The temperature gradient is presented in Table 5 and Figure 3.

Table 5 - Temperature Gradient in the Liquid Hydrogen Strut During Coast, Conduction Only

Length, inches	Temperature, °R.
0.000	37
0.382	60
0.615	72
1.252	100
2.68	150
4.45	200
6.52	250
8.86	300
11.95	360
14.11	400
19.93	500
21.77	530

The temperature gradient of about 0.8°F. in the cold titanium end fitting has been neglected in these calculations.

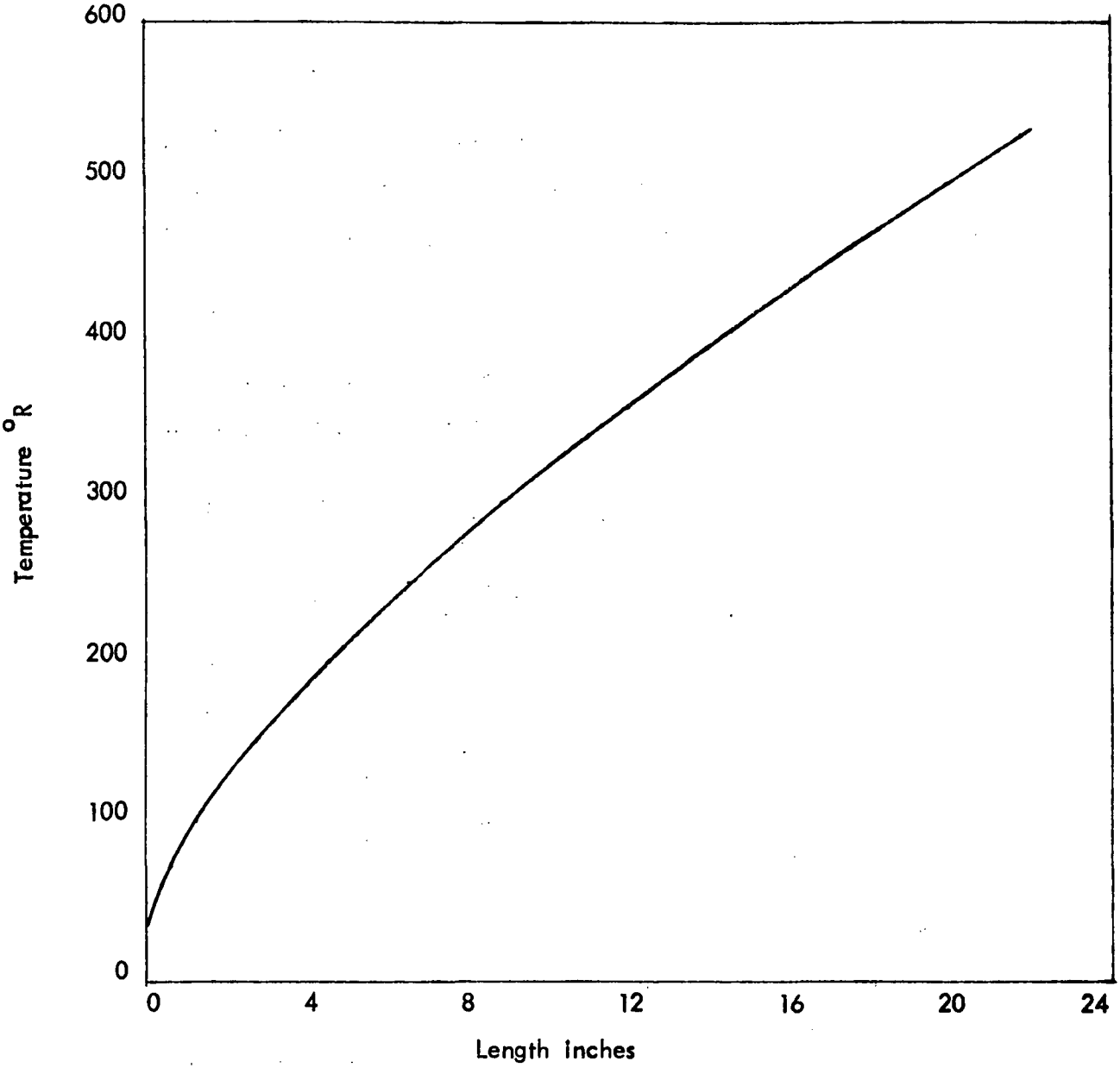

Figure 3. Temperature of Hydrogen Strut, Conduction Only, during Coast

3.2 RADIATION

The radiation heat transfer for the hydrogen strut has been calculated using handbook values of emissivities and appropriate shape or view factors. These calculations have considered the maximum heat transfer with no radiation shields, effects of plating the ends of the struts, and effects of multiple radiation barriers within the strut.

The following emissivity values were used: (Ref. 7)

Titanium at 530°R	0.14
Titanium at 37°R	0.05
Gold or aluminum	0.018
Epoxy-glass strut	1.00

Shape factors for radiation directly from end to end of a cylinder have been published by two authorities in slightly different form (Ref. 7, 8). For opposite disks of equal radius, both equations reduce to:

16. $$F_{12} = 1/2 \left[2 + \frac{L^2}{R^2} - \sqrt{\frac{L^4}{R^4} + \frac{4L^2}{R^2}} \right]$$

The radiation from an end to the side wall is simply: $F_{1W} = 1 - F_{12}$.

View factors of the hydrogen strut are plotted in Figure 4.

The several resistances to radiative heat transfer may be noted as follows:

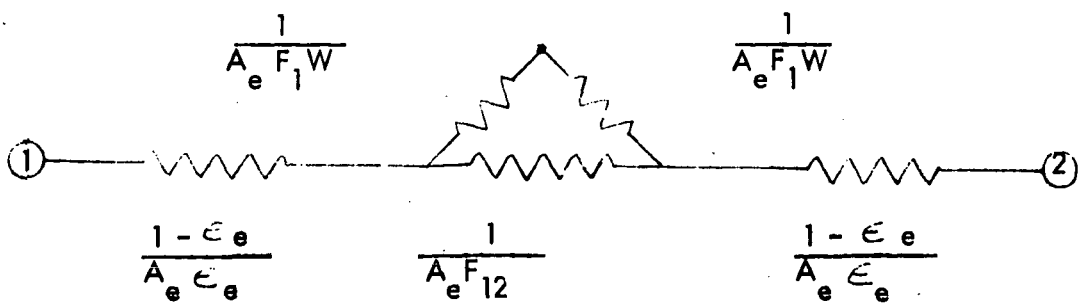

Where ϵ_e = emissivity at the end fitting
Ae = area of the end fitting

Figure 4. Radiation View Factors of Hydrogen Strut as Function of Distance

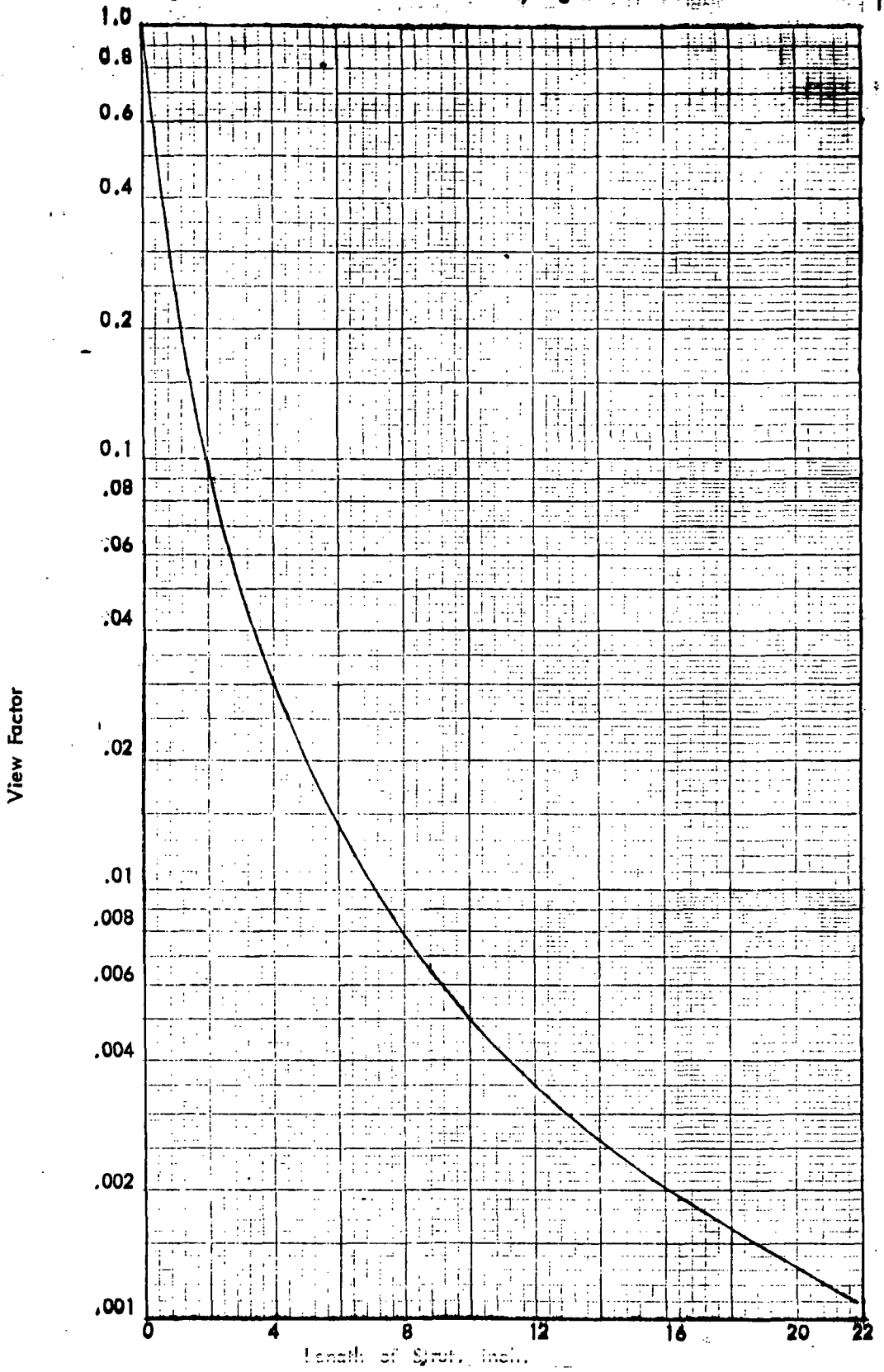

The combined effects of axial radiation and radiation to the walls will contribute to the total heat transfer. At the warm end fitting of the -1 strut the radiant transfer has been calculated as a function of location for the first radiation barrier. The above resistance network was used for this calculation along with a Te of 530°R and wall temperature distribution as noted in Table 5 and Figure 3. The end-fitting emissivity was assumed to be $\epsilon_e = 0.14$ (clean titanium) or $\epsilon_e = 1.0$ (dirty extreme). Barrier emissivity was selected as 0.02. Results of these calculations are noted in Table 6.

For the total radiant contribution to heat transfer must be less than .0057 Btu/hr., a clean titanium end fitting is imperative and the first radiation barrier must be within 0.8 inches, noted in Figure 5. A closer spacing should be expected, since other components of the strut provide radiative contributions.

A second radiation barrier of emissivity 0.02 can be assumed, and transfer is afunction of distance approximately 1/7 that noted for $\epsilon_e = 0.14$ in Table 6. At a spacing of 1 inch from the first barrier, secondary radiative transfer would be about 0.001 Btu/hour. Of course this must be added to the first increment of radiative transfer, and the sum of all such increments must not exceed .0057 Btu/hour.

Intuitively, a total of about 20 radiation barriers would be required for the hydrogen strut. This poses a difficult assembly task.

Another approach to the radiation problem has been considered. This involves filling the interior of each strut with an opaque, low-conductivity material. Candidate materials include perlite (not completely opaque at 7.5 micron), calcium silicate (Johns-Manville Microcell or Microcellate), carbon black (Great Lakes Carbon Nerofil) and aluminized Mylar. Values of thermal conductivities in the range of 530 to 140°R have been published for most of these materials, where radiation transfer is included in the total conductivity. These values and the calculated internal transfer for the hydrogen strut are shown in Table 7.

Table 6 - Radiation from Warm End Fitting To Strut and to Barrier

q1w = radiation, end fitting to wall, Btu/hr.
qw2 = radiation, wall to radiation barrier, Btu/hr.
q12 = radiation, end fitting to radiation, Btu/hr.
D = distance from end fitting to barrier, inch.

D	q 1 w		q w 2	q 1 2		q total	
	$\epsilon_e = 1.0$	$\epsilon_e = 0.14$		$\epsilon_e = 1.0$	$\epsilon_e = 0.14$	$\epsilon_e = 1.0$	$\epsilon_e = 0.14$
0.5	.0118	.00165	.0004	.0013	.0002	.0135	.0022
1.0	.0464	.0065	.0009	.0008	.0001	.0481	.0075
2.0	.123	.0172	.0025	.0007	.0001	.126	.020

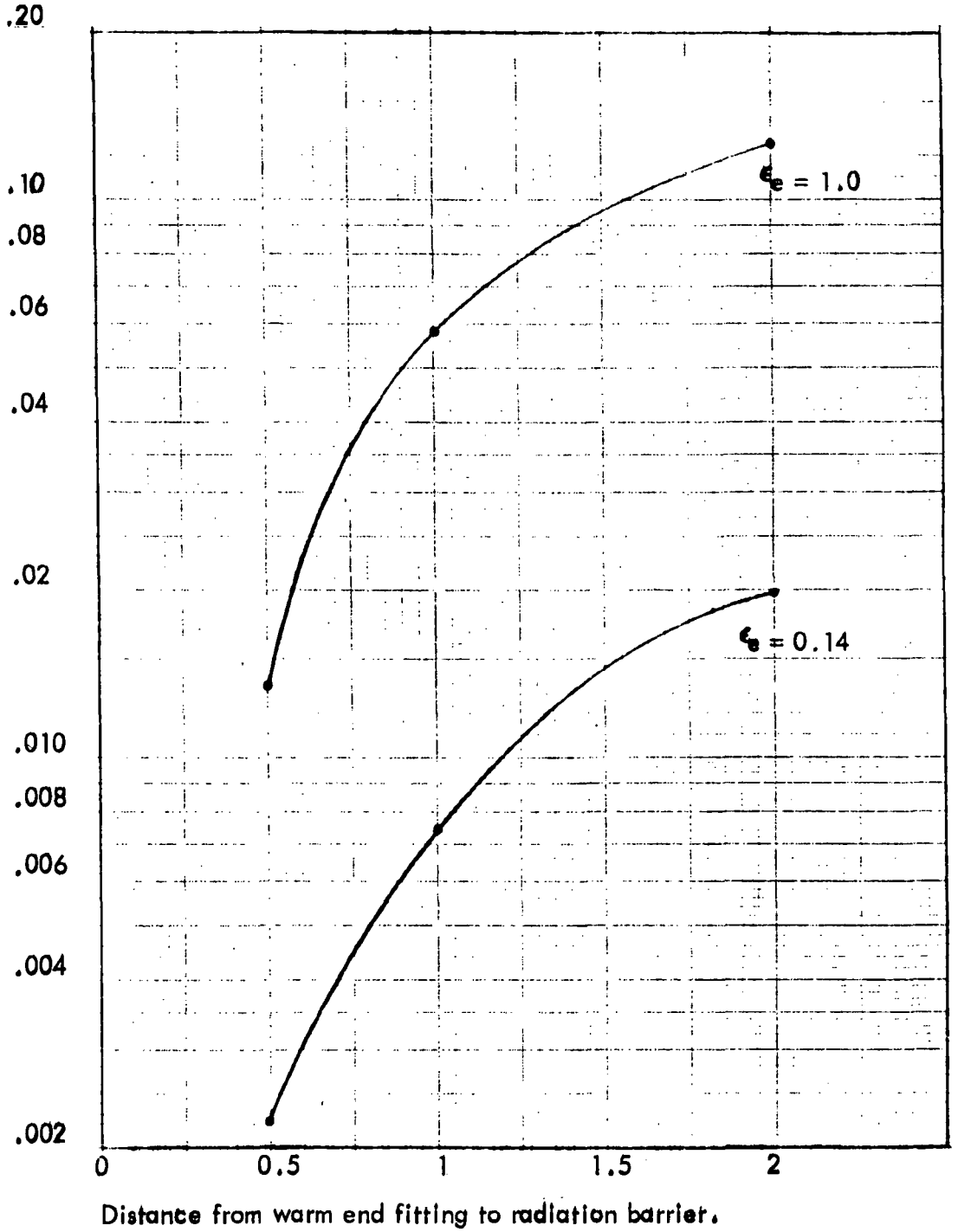

Figure 5 - Radiant Heat Transfer from Warm End Fitting To Strut with Radiation Barrier (ϵ = .02)

Table 7 -- Thermal Conductivities and Internal Heat Transfer of Prospective Insulating Systems in Vacuum

Material	Density pcf	Thermal Conductivity Btu/hr ft °F.	Transfer in Hydrogen strut Btu/hr	Reference
Perlite	2	.0010	.00308	Kropschot, 11
	6	.00070	.00215	"
Calcium silicate	21.4	.00032	.00098	Fulk, 12
Carbon Black	12	.00035	.00108	Kropschot, 13
Chopped aluminized Mylar	1 - 2	.00003		Perry, 14
Opacified Perlite	6	.00050	.00154	Kropschot, 11

Kropschot (11) recommends against using perlite in a helium environment because of both adsorption and absorption on silica; this could cause excessive heat transfer during early parts of the coast period since helium would evacuate slowly. The calcium silicate and carbon black also have high surface areas and would desorb helium slowly. During the period of desorption the effective thermal conductivity of the powder/gas mixture would be equal to the gas conductivity, which is 7.2×10^{-2} for helium.

3.3 RADIATION CRITIQUE

The above analyses indicate that sufficiently low radiative heat transfer can be accomplished with either multiple radiation barriers or with an opaque powder. The barriers have placement problems, the powders have absorption and dusting problems.

An approximation to the radiation barrier effect can be accomplished by using aluminized mylar and Dexiglass in cut flakes 1/4" to 1/2" square. This material can be placed at a density about 1 pcf. By using two layers of Dexter paper #X1303 (13.74 gm/sq meter) and one layer of aluminized 0.25 mil Mylar (9.12 gm/sq) the 1 pcf insulation provides 466 sq inches of aluminized radiation barrier in the hydrogen strut. This is 264 times the cross-section area

or about 130 effective disks. Internal heat transfer in the hydrogen strut during coast is 1.0×10^{-4} Btu/hr if the effective conductivity of the glass paper/aluminized Mylar is 3×10^{-5} as noted in Table 7.

This insulation is recommended for all three cryogenic struts of this study.

4. CONVECTIVE ENVIRONMENTS

The pre-launch environment of the struts presumes a free circulation of helium gas. The heat transfer from helium convection is partly dependent upon the circulation patterns surrounding the struts and may also be highly dependent upon convection patterns from the large cryogenic tanks.

4.1 CONVECTIVE EQUATIONS

The struts have been considered independent of external equipment using the standard equations for free convection of gases adjacent to vertical surfaces (Ref. 15):

For film Reynolds number exceeding 10,000

17. $j = (h/cG)\,(c\mu/k)^{2/3} = 0.13/(LG/\mu)^{1/3}$

For film Reynolds number 100 to 10,000

18. $j = (h/cG)\,(c\mu/k)^{2/3} = 0.59/(LG/\mu)^{1/2}$

Where G = mass film velocity $= (gB\Delta t\, \rho^2 L)^{1/2}$

$g = 4.18 \times 10^8$ ft/hr^2

$B = .0025/^{\circ}R$

$t = (400 - T_w)\ ^{\circ}R$

$\rho = .01370$ lb/cu.ft.

L = strut length (1.09 ft., 1.34 ft., 0.84 ft. for H_2 FLOX, CH_4)

h = film coefficient, Btu/sq ft hr $^{\circ}F$

$c = 1.2480$ Btu/lb.

$\mu = 0.155$ centipoise $= 0.0375$ lb/hr ft

$k = .0714$ Btu fr/hr sq ft$^{\circ}F$

Reynolds Number, $Re = LG/\mu = 373\, L^{3/2}\,(400-T)^{1/2}$

For the -1 hydrogen strut the Reynolds number exceeds 10,000 for $T_w < 310^{\circ}R$ and is less than 10,000 for warmer temperatures. For the FLOX and methane struts, the Reynolds number is always less than 10,000.

Results from convective heat transfer calculations are presented in Table 8.

Table 8 - Convective Heat Transfer Coefficients

Strut Temperature T_w °R.	Eqn.	Heat Transfer Coefficient, h, Btu/hr. sq. ft. °F		
		-1 strut	-2 strut	-3 strut
36	17	1.72		
72	17	1.64		
100	17	1.59		
150	17	1.50		
150	18		2.82	
200	17	1.39		
200	18		2.66	3.00
250	17	1.26		
250	18		2.48	2.79
300	17	1.10		
300	18	2.03	2.24	2.52
350	18	1.71	1.88	2.12
400	18	0	0	0
Average		1.71	2.71	3.0

The calculations for hydrogen strut presented an insight into the approximations of natural convection equations. At the Reynolds number cross-over point (10,000 corresponding to about 300°R) equations 17 and 18 gave answers differing by a factor of two. Since convective transfer equations have a precision not better than +100% - 50% the average values of the above coefficients have been accepted for further calculations.

4.2 THERMAL CONDUCTIVITY OF THE STRUTS

The composite analysis of the -1 hydrogen strut has been discussed in section 3.1, page 9. The other struts are similarly described below using the same properties of glass and resin:

7. $K_g = 0.0699 + 1.739 \times 10^{-3} T - 1.440 \times 10^{-6} T^2$

8. $K_r = 0.0192 + 3.831 \times 10^{-4} T - 4.035 \times 10^{-7} T^2$

The -1 hydrogen strut has an axial conductivity, as follows:

19. $K = 0.337\ K_g + 0.1634\ K_r + K_g K_r / (2.019\ K_r + 0.981\ K_g)$

Cross-section area of the fiberglass is 9.62×10^{-4} sq. ft.

If helium can flow freely within the strut, the internal heat transfer would be due to $K_{He} = 0.072$ and $A_{He} = 0.113$. External convection would result from $h = 1.71$ and $dA = 0.393\ dL$.

The differential equation describing simultaneous conduction and convection is:

$$20.\quad \frac{(9.62 \times 10^{-4}\ K + 7.42 \times 10^{-4})}{T - 400}\quad d^2T = 0.393\ dL^2$$

This equation is integrated twice using boundary conditions $L = 0$ at $T = 400^{\circ}R$. and $L = 1.81$ at $T = Ta$.

The -2 FLOX strut has a conductivity:

$$21.\quad K = 0.302\ K_g + 0.147\ K_r + K_g K_r / (1.682\ K_r + 0.817\ K_g)$$

Area of this strut is 0.00191 sq. ft. Internal helium convection area is 0.01485 sq. ft. External convection coefficient is 2.71 with external area $dA = 0.458\ dL$. This strut has the following differential equation for simultaneous conduction and convection:

$$22.\quad \frac{(.00191\ K + .00107)}{T - 400}\quad d^2T = 1.24\ dL^2$$

Boundary conditions are $L = 0$ at $T = 400$, $L = 1.130$ at $T = Ta$.

The -3 methane strut has a conductivity:

$$23.\quad K = 0.337\ K_g + 0.1634\ K_r + K_g K_r / (2.019\ K_r + 0.981\ K_g)$$

Area of this strut is 9.62×10^{-4} sq. ft. Internal helium convection area is 0.0113 sq. ft. External convection coefficient is 3.00 and external area, $dA = 0.393\ dL$. This strut has the following differential equations for simultaneous conduction and convection:

$$24.\quad \frac{(9.62 \times 10^{-4}\ K + 7.42 \times 10^{-4})}{T - 40}\quad d^2T = 1.18\ dL^2$$

Boundary conditions are $L = 0$ at $T = 400$, $L = 0.791$ at $T = Ta$.

Results from the above integrations coupled with end-fitting temperature gradients are presented in Table 9.

4.3 TEMPERATURE GRADIENTS AT COLD END FITTINGS

Where helium convection occurs, heat transfers rather rapidly from the warm gas to the glass/epoxy wrappings around the titanium end fittings. The temperature gradients in this area have been calculated using an assumed spool geometry of the titanium fitting as shown in Figure 6 and Table 9.

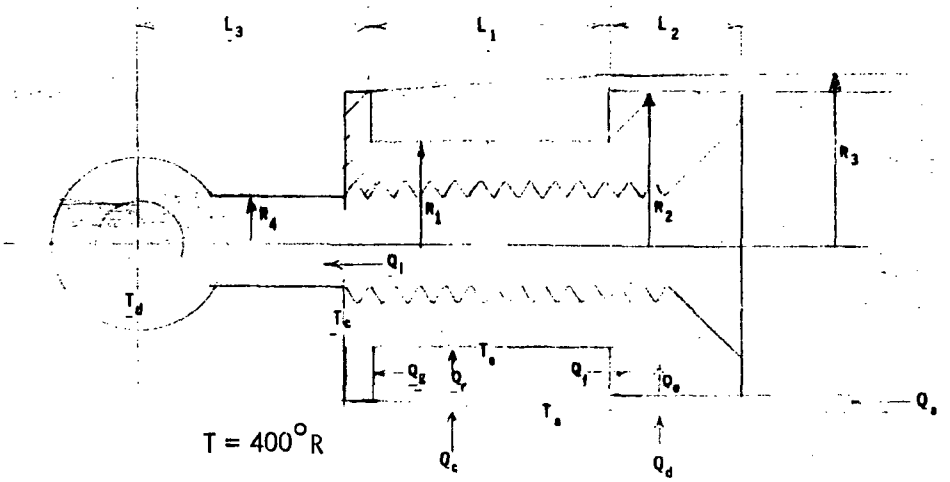

Figure 6. End-Fitting Approximation for Calculating Temperature Gradients.

Table 9 - End - Fitting Dimensions and Parameters

	Strut		
	-1	-2	-3
R_1, ft.	.030	.0416	.030
R_2, ft.	.062	.075	.062
R_3, ft.	.066	.079	.066
R_4, ft.	.020	.025	.020
L_1, ft.	.039	.056	.039
L_2, ft.	.032	.029	.032
L_3, ft.	.083	.100	.083
Td, °R	36	155	204
h, Btu/hr.sq.ft.°F	1.71	2.71	3.0
Ke, Btu/hr.sq.ft.°F	.1214	.167	.130
Kr, Btu/hr.sq.ft.°F	.0832	.150	.170
Kt, Btu/hr.sq.ft.°F	1.60	2.65	3.04
Ks, Btu/hr.sq.ft.°F	3.20	5.30	6.10

Heat conduction through the simplified end-fitting geometry can be described with 14 unknowns and equations along with four lucky guesses. First approximations must be made of the axial heat transfer, Q_a, and warm-end temperature gradient.

In addition to the differential equations for strut temperature distribution (20, 22 and 24) the following simultaneous equations derive from end-fitting heat transfer:

25. $Qa + Qd = Qe + Qb$

26. $Qb + Qc = Qr + Qf + Qg$

27. $Ql = Qr + Qe$

28. $Qd = 2 \quad R_3 L_2 h (400 - Ta)$

29. $Qe = \dfrac{2 \quad R_3 L_2 ke (Ta - Tb)}{R_3 - R_2}$

30. $Qc = 2 \quad R_2 L_1 h (400 - Ta)$

31. $Qr = 2 \quad Kr L_1 \dfrac{(R_1 + R_2)}{2} \quad \dfrac{(Ta + Te)}{(R_2 - R_1)}$

32. $Qf = \dfrac{4 \quad Kr (R_2^2 - R_1^2)}{L_1} \quad \left(\dfrac{Ta + Te}{2} - Tb\right)$

33. $Qg = \dfrac{4 \quad Kr (R_2^2 - R_1^2)}{L_1} \quad \left(\dfrac{Ta + Te}{2} - Tc\right)$

34. $Qe = 0.080 \; Kt \; (Tb - Te)$

35. $Qi = 0.085 \; Kt \; (Te - Tc)$

36. $Ql = - \quad R_4^2 \; Ks \dfrac{dT}{dL} \quad @ \; T = Tc$

37. $\dfrac{R_4^2 \; Ks \; d^2T}{(T - 400)} = 2 \quad R_4 h \, dL^2$

$T = Tc \; @ \; L = 0$
$T = Td \; @ \; L = L_3$

Results of a third iteration of these calculations are shown in Table 10. Temperature gradients in struts are shown in Table 11 and Figure 7. The convective environment from helium at 400°R overwhelms the conduction and radiation heat transfer. The maximum radial temperature gradient is 37.5°F/inch, and the maximum axial temperature gradient is in the hydrogen strut, 270°F/inch, at the cold end.

Table 10 - Temperature Gradients in End-Fittings

	Strut		
	-1	-2	-3
q_a, axial heat transfer, Btu/hr.	3.41	3.95	2.75
qi, transfer to fitting, Btu/hr.	6.28	8.38	5.94
T_a, external composite, °R	263.3	310.7	317.4
T_b, titanium bell, °R	261.5	309.5	316.4
T_e, titanium shank, °R	255.9	306.0	313.9
T_d, cryogen, °R	37	155	204
Gradient $(T_a - T_b) / (R_3 - R_2)$ °R/inch	37.5	25.0	20.8
Gradient $(T_a - T_e) / (R_2 - R_1)$ °R/inch	19.3	11.8	9.1

Table 11 - Axial Temperature Gradient in Struts During 400°R Helium Convection

Strut Temperature °R.	Length of Strut from warm end, ft.		
	-1	-2	-3
400	0	0	0
395	1.68	1.02	0.705
390	1.71	1.05	0.728
380	1.735	1.08	0.748
370	1.75	1.09	0.761
360	1.76	1.10	0.770
350	1.77	1.11	0.776
317.4			0.791
310.7		1.13	
300	1.80		
263.3	1.81		

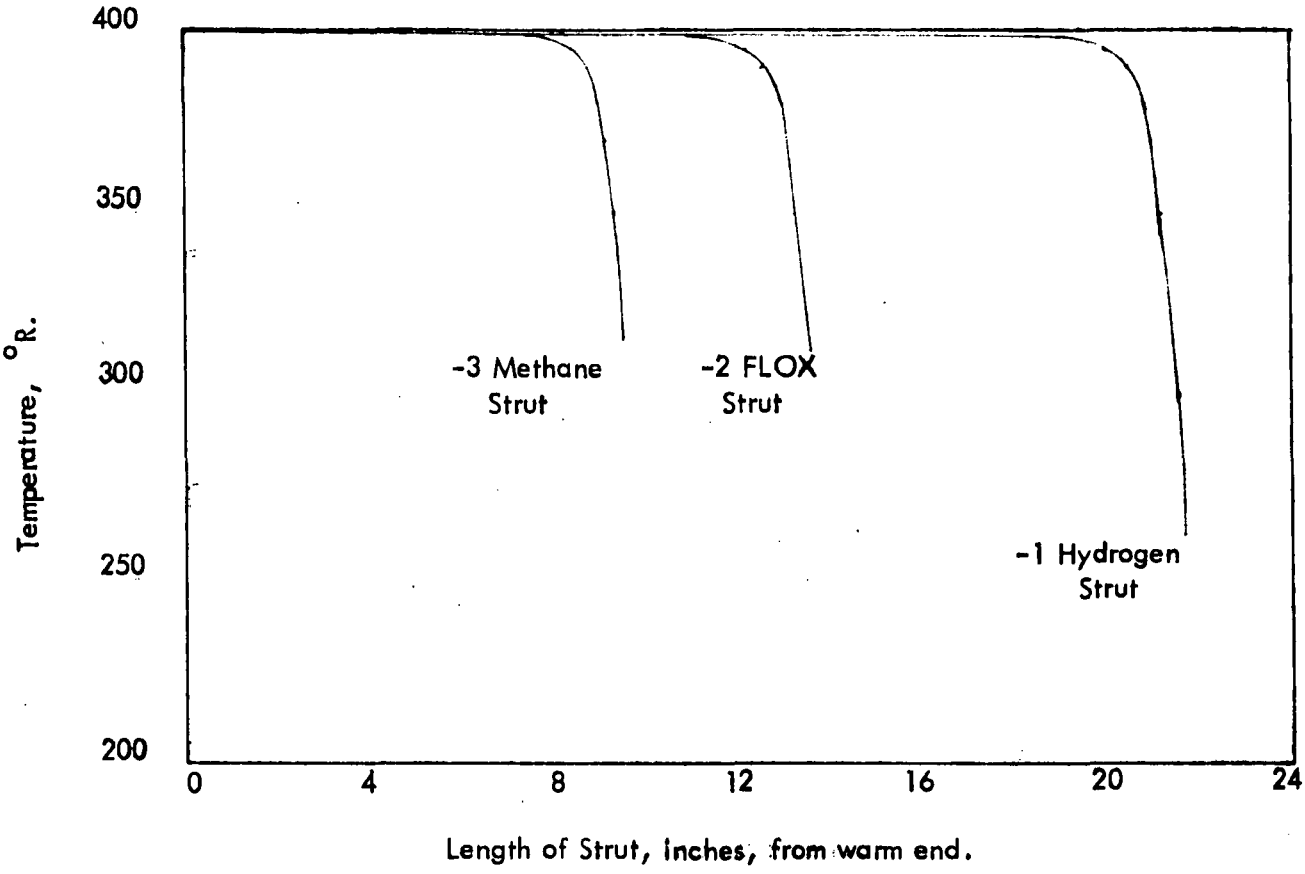

Figure 7 - Temperature Gradients in Struts During Convection

REFERENCES

1. J. G. Hust and R. L. Powell "Thermal Conductivity of Aerospace Alloys at Cryogenic Temperatures", page 200 of C. Y. Ho and R. E. Taylor, editors, Thermal Conductivity Proceedings, 8th Conference, Purdue University, October, 1968.

2. R. W. B, Stephens, "The Temperature Variation of the Termal Conductivity of Pyrex Glass", Philosophical Magazine, vol. 14, pp 897-914 (1932).

3. G. K. White, "Measurement of Solid Conductivities at Low Temperatures", page 86 of R. P. Tye, editor, Thermal Conductivity, vol. 1, Academic Press, New York, 1969.

4. "Design and Fabrication of Shadow Shield Systems for Thermal Protection of Cryogenic Propellants", Contract NAS 3-10292, NASA CR 72595, page 29, Arthur D. Little, Inc., Nov. 27, 1969.

5. J. F. Haskins, M. D. Campbell, J. Hertz and J. L. Percy, "Thermophysical Properties of Plastic Materials and Composites to Liquid Hydrogen Temperature", pp 71-72, General Dynamics Astronantics, San Diego, Contract AF 33(657)-9160, Report ML-TDR-64-33 Part 1, June 1964 (AD 601337).

6. B. R. Bullard, "Cryogenic Tank Support Evaluation", NASA CR 72546 page 41, Lockheed Missile & Space Company, final report December 1, 1969, Contract NAS 3-7979.

7. J. P. Dobbins, "Emittance of Oxidized Metals", North American Aviation, Inc., Los Angeles. ASME Paper 50-A-58, November 1950.

8. F. Kreith, Radiation Heat Transfer, International Textbook Company, Scranton, Pa. 1962.

9. H. C. Hottel & A. F. Sarofim, Radiative Transfer, Mc Graw - Hill, New York 1967.

10. C. W. Keller, "Fiberglass Supports for Cryogenic Tanks", 12th monthly report, Contract NAS 3-12037, May 1970, Lockheed Missile & Space Co.

11. R. H. Kropschot and R. W. Burgess, "Perlite for Cryogenic Insulation", K. D. Timmerhans, editor, Advances in Cryogenic Engineering, vol. 8, pp 425-436, Plenum Press, New York, 1963.

12. M. M. Fulk, "Evacuated Powder Insulation for Low Temperatures", in K. Mendelssohn, editor, Progress in Cryogenics, vol. 1, pp 65-84, Academic Press, New York 1959.

13. R. H. Kropschot, "Low Temperature Insulation", in R. W. Vance and W. M. Duke, editors, Applied Cryogenic Engineering, page 161, John Wiley, New York, 1962.

14. J. L. Perry, "Cryostat Design", in H. Weinstock, editor, Cryogenic Technology, Page 59, Boston Technical Publishers, Cambridge, Mass. 1969.

15. J. H. Perry, editor, Chemical Engineers' Handbook, page 10, Mc Graw - Hill, New York, 1963.

APPENDIX B

DISTRIBUTION LIST

DISTRIBUTION LIST

COPIES	RECIPIENT	DESIGNEE
	National Aeronautics & Space Administration Lewis Research Center 21000 Brookpark Rd. Cleveland, OH 44135	
1	Attn: Contracting Officer, MS 500-312	
1	Attn: Technical Report Control Office, MS 5-5	
1	Attn: Technology Utilization Office, MS 3-16	
1	Attn: Library, MS 60-3	
1	Attn: D. L. Nored, MS 500-203	
1	Attn: H. W. Douglass, MS 500-203	
1	Attn: E. W. Conrad, MS 500-204	
1	Attn: A. V. Zimmerman, MS 501-2	
1	Attn: W. G. Anderson, MS 501-2	
1	Attn: H. H. Valentine, MS 501-2	
1	Attn: J. R. Barber, MS 500-209	
1	Attn: R. H. Johns, MS 49-1	
1	Attn: Patent Office, MS 500-311	
5	Attn: B. Linscott, MS 501-2	
2	Chief, Liquid Propulsion Technology, RPL Office of Advanced Research and Technology NASA Headquarters Washington, DC 20546	
1	Director, Technology Utilization Division Office of Technology Utilization NASA Headquarters Washington, DC 20546	

COPIES	RECIPIENT	DESIGNEE
1	Aerospace Corporation 2400 East El Segundo Boulevard P.O. Box 95085 Los Angeles, California 90045	John G. Wilder MS-2293
2	Boeing Company P. O. Box 3707 Seattle, Washington 98124	D. H. Bartlett
1	Missile Division Chrysler Corporation P.O. Box 2628 Detroit, Michigan 48231	John Gates
2	General Dynamics, Convair Division Library & Information Services (128-00) P. O. Box 1128 San Diego, California 92112	Ross S. Ringwald
1	Missile & Space Systems Division McDonnell-Douglas Aircraft Company 3000 Ocean Park Boulevard Santa Monica, California 90406	R. W. Hallet Chief Engineer Adv. Space Tech.
1	Space & Information Systems Division North American Rockwell 12214 Lakewood Boulevard Downey, California 90241	Library
1	Grumman Aircraft Engineering Corp. Bethpage, Long Island, New York 11714	George R. Pinter
2	Lockheed Missiles and Space Co. Attn: Technical Information Center P. O. Box 504 Sunnyvale, California 94088	C. W. Keller
1	Martin Marietta Corporation Baltimore Division Attn: Library Baltimore, Maryland 21203	
1	Martin Marietta Corporation Denver Division Attn: Library P. O. Box 179 Denver, Colordao 80201	
1	Martin Marietta Corporation Orlando Division Box 5827 Orlando, Florida 32800	

COPIES	RECIPIENT	DESIGNEE
3	NASA Scientific & Technical Information Facility P. O. Box 33 College Park, Maryland 20740	
1	Goddard Space Flight Center Greenbelt, Maryland 20771	Merland L. Moseson Code 620
1	Jet Propulsion Laboratory California Institute of Technology 4800 Oak Grove Drive Pasadena, California 91103	Henry Burlage, Jr. Propulsion Div., 38
	Langley Research Center Langley Station Hampton, Virginia 23365	Ed Cortwright Director
2	Marshall Space Flight Center Huntsville, Alabama 35812	Hans G. Paul Code R-P&VED
2	Manned Spacecraft Center Houston, Texas 77001	Joseph G. Thibodaux, Jr. Chief, Propulsion & Power Division
1	Aeronautical Systems Division Air Force Systems Command Wright-Patterson Air Force Base Dayton, Ohio 45433	D. L. Schmidt Code ASRCNC-2
1	Space and Missile Systems Organization Air Force Unit Post Office Los Angeles, California 90045	Col. Clark Technical Data Center
1	Bureau of Naval Weapons Department of the Navy Washington, DC 20546	J. Kay RTMS-41
1	Defense Documentation Center Headquarters Cameron Station, Building 5 5010 Duke Street Alexandria, Virginia 22314 Attn: TISIA	
1	Chemical Propulsion Information Agency Applied Physics Laboratory 8621 Georgia Avenue Silver Springs, Maryland 20910	Tom Reedy